

Properties of exopolymeric substances (EPS) produced during cyanobacterial growth: potential role in whitening events

Marlisa Martinho de Brito^{1*}, Irina Bundeleva¹, Frédéric Marin¹, Emmanuelle Vennin¹, Annick Wilmotte², Laurent Plasseraud³ and Pieter T. Visscher^{1,4}.

¹Biogeosciences Laboratory, Department of Life, Earth and Environmental Sciences, University of Bourgogne Franche-Comté, 21000 Dijon, France

²InBios Research Unit, Department of Life Sciences, Faculty of Sciences, University of Liège, 4000 Liège, Belgium

³ICMUB Institute of Molecular Chemistry (CNRS UMR CNRS 6302), University of Burgundy-Franche-Comté, 21000 Dijon, France

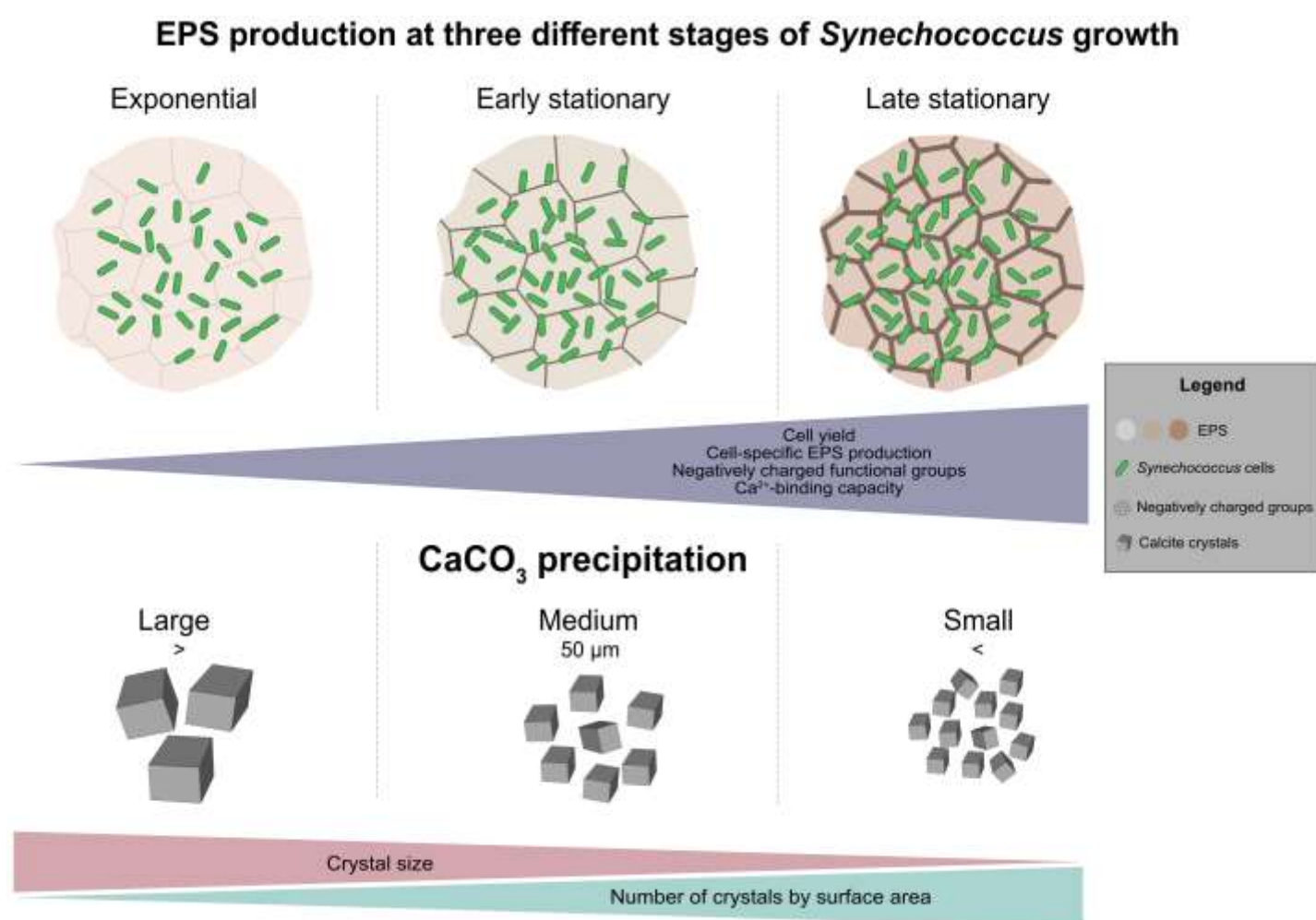
⁴Department of Marine Sciences, The University of Connecticut, Groton, CT 06340, USA

Correspondence to: Marlisa Martinho de Brito (marlisa_de-brito@etu.u-bourgogne.fr)

Abstract

Extracellular polymeric substances (EPS) are an important organic carbon reservoir in many pelagic and benthic environments. The production of EPS is intimately associated with the growth of phyto- and picoplankton. EPS plays a critical role in carbonate precipitation through the binding of cations and by acting as a nucleation site for minerals. Large-scale episodes of fine-grained calcium carbonate precipitation in the water column (whiting events) have been linked to cyanobacterial blooms, including of *Synechococcus* spp.. The mechanisms that trigger these precipitation events are still debated. We pose that the cyanobacterial EPS, produced during exponential and stationary growth phases plays a critical role in the formation of whittings. The aim of this study was to investigate the production of EPS during a two-month cyanobacterial growth, mimicking a bloom. The production and characteristics of EPS were examined in different growth stages of *Synechococcus* spp. using various techniques such as FT-IR spectroscopy, colorimetric and SDS-PAGE assays. We further evaluated the potential role of EPS in carbonate precipitation through *in vitro* forced precipitation experiments. EPS produced during the early and late stationary phase contained a larger amount of negatively charged groups than present in EPS produced during the exponential phase. Consequently, a higher Ca²⁺ binding affinity of the stationary phase-EPS led to the formation of a larger amount of smaller carbonate minerals (<50 μm) compared to crystals formed in exponential phase-EPS, which were less abundant and larger (> 50 μm). These findings were used to establish a conceptual model for picoplankton bloom-mediated CaCO₃ precipitation that can explain the role of EPS in whittings (see graphical abstract).

Graphical abstract



1. Introduction

1.1 Significance of this study

Massive carbonate precipitation episodes in the water column, also referred to as 'whiting events' are a well-known phenomenon of modern freshwater (Schultze-Lam et al., 1997; Hodell et al., 1998; Stanton et al., 2021) and marine environment (Shinn et al., 1989; Robbins and Blackwelder, 1992; Larson and Mylroie, 2014). Whittings are caused by large-scale precipitation of micron-sized calcium carbonate particles (visible from space) and represent a major sink in the carbon cycle. The particles associated with whittings can make up a major sedimentary constituent of the modern-day and ancient carbonate rock records (Pomar and Hallock, 2008). Whiting events can be triggered by a combination of biological and physicochemical processes. Among the biological mechanisms that have been studied in this context, picocyanobacterial proliferations have often been invoked in the initiation of whittings (Hodell et al., 1998; Thompson, 2000; Obst et al., 2009). Photosynthesis increases pH levels and alkalinity during cyanobacterial blooms, ultimately causing the saturation state of calcium carbonate to rise, thereby leading to its potential precipitation. The role of *Synechococcus* spp. bloom-forming cyanobacteria in CaCO₃ precipitation has been demonstrated in laboratory experiments (Yates and Robbins, 1998; Dittrich et al., 2003; Obst et al., 2009; Bundeleva et al., 2014; Martinho de Brito et al., 2022) and observed in field investigations (Wells and Iling, 1964; Thompson et al., 1990; Dittrich and Obst., 2004). Change in temperature, salinity, CO₂ pressure as well as turbulence are some of the physicochemical factors

44 that can lead to the formation of supersaturated solutions and subsequent precipitation of CaCO₃ thus initiating the whiting. Even though several possible biogenic
45 and abiotic mechanisms have been identified, the formation of whittings is still poorly understood.

46 1.2 Overview of phytoplankton blooms

47 Phytoplankton blooms, including those of picoplankton, are dense accumulations of cells resulting in a visible discoloration of the surface water layers (Reynolds and
48 Walsby, 1975; Huisman et al., 2018). Their occurrence has been recorded worldwide in marine and freshwater bodies (Paerl et al., 2001; Paerl and Huisman, 2008;
49 Ploug, 2008). Light intensity, water temperature, nutrient availability, weather conditions and hydrodynamics are key factors that determine the onset and persistence
50 of a bloom. Blooms are typically seasonal, frequently observed during late spring or summer, and can be dominated by picoplankton (Huisman et al., 2018). Some
51 phytoplankton organisms, notably cyanobacteria, may produce toxins and form large-scale harmful algal blooms (Paerl et al., 2001). The intensity and frequency of
52 cyanobacterial blooms have been increasing due to anthropogenic eutrophication (Heisler et al., 2008; O'Neil et al., 2012), a trend expected to exacerbate due to
53 climate change (Lüring et al., 2018). Cyanobacteria comprise a diverse group of photoautotrophic organisms that play a pivotal role in global primary production and
54 are key players in the biogeochemical cycles of carbon, nitrogen and oxygen (Callieri and Stockner, 2000; Raven et al., 2017). The unicellular cyanobacterium
55 *Synechococcus* is one of the most abundant photosynthetic microorganisms on Earth (Whitton and Potts, 2012), which contribute substantially to the picoplankton
56 community in marine (Murphy and Haugen, 1985; Coello-Camba and Agustí, 2021) and freshwater environments (Weisse, 1993) that can form dense blooms
57 (Schultze-Lam et al., 1992; Philips et al., 1999; Dittrich and Obst, 2004).

58 1.3 Phytoplankton blooms and CaCO₃ precipitation

59 During the occurrence of dense phytoplankton blooms, high rates of photosynthetic activity lead to a rapid depletion of CO₂ in the surface waters, increasing alkalinity.
60 Depending on the buffering capacity of the water, this could result in pH values ≥ 9 to as high as 11 (Ibelings and Maberly, 1998; Zepernick et al., 2021). Consequently,
61 the inorganic carbonate equilibrium shifts towards carbonate (CO₃²⁻). Some cyanobacteria possess a carbon concentrating mechanism (CCM) that converts HCO₃⁻ to
62 CO₂ through the action of carbonic anhydrase enzymes (Price et al., 1998; Badger et al., 2002) and produce hydroxide ions (Kupriyanova and Pronina, 2011). The
63 activity of extracellular carbonic anhydrase (eCA) may contribute to the create an alkaline microenvironment in the extracellular polymeric substances (EPS)
64 surrounding the cyanobacterial cells (Price et al., 2002; Dupraz et al., 2009). When OH⁻ ions are released during photosynthesis it causes the pH to rise, which favors
65 carbonate mineral precipitation, assuming there are enough calcium ions available (Kamennaya et al., 2012). Consequently, during blooms, carbonate minerals can
66 form on EPS or precipitated in the microenvironment surrounding cyanobacterial cells.

67 1.4 The role of EPS

68 Cyanobacteria are known producers of EPS, especially during blooms (Pannard et al., 2016; Liu et al., 2018). EPS serve as a boundary between cells and their
69 immediate environment (Whitton and Potts, 2012) and may act as a template for CaCO₃ nucleation (Dupraz and Visscher, 2005; Dupraz et al., 2009; Kamennaya et
70 al., 2012). EPS are high molecular weight organic molecules composed of polysaccharides, proteins, nucleic acids and lipids (Pereira et al., 2009; Marvasi et al., 2010;
71 Decho and Gutierrez, 2017). This complex mixture of molecules may contain specific monomer components, such as uronic or sialic acids (monosaccharides), aspartic
72 or glutamic acids (amino acids) or functions (sulfate, phosphate), which carry negative charges in physiological conditions and can therefore bind cations, such as
73 Ca²⁺, and promote the nucleation of CaCO₃ crystals (Trichet and Defarge, 1995; Dupraz et al., 2009; Walker et al., 2019). Conversely, polyanionic EPS in solution
74 can inhibit crystal growth by poisoning the faces of growing nuclei by an adsorption mechanism, according to a classical and accepted view prevailing for other
75 macromolecules of similar charge properties: synthetic peptides (Wheeler et al., 1991), skeletal proteins (Wheeler et al., 1981; Addadi and Weiner, 1985), coccolith-
76 associated polysaccharides (Borman et al., 1982) or natural organic matter dissolved in seawater (Mitterer and Cunningham, 1985). The production and composition
77 of EPS differ among different species of microorganisms and their type of metabolism and depend on environment in which they live, stressors (e.g., nutrient
78 availability, pH, temperature, light, salinity) and the stage of their growth (Pereira et al., 2009; Pannard et al., 2016; Martinho de Brito et al., 2022). The deprotonation
79 of functional groups at elevated pH enhances the binding capacity of cations such as Ca²⁺ and controls crystal nucleation and growth by reducing the interfacial energy
80 barrier between the crystal and the EPS substrate (Dupraz et al., 2009; Dittrich and Sibling, 2010). EPS play a two-fold role in carbonate formation by initially inhibiting
81 (through Ca²⁺ binding) and subsequently promoting carbonate precipitation by releasing calcium ions during EPS alteration and degradation (Dupraz and Visscher,
82 2005). Furthermore, through specific functional group composition and structural architecture, EPS may also exert control over the mineralogy, morphology and/or
83 abundance of the minerals that are formed (Trichet and Defarge, 1995; Dupraz et al., 2009).

84 1.5 The goal of this study

85 We have previously reported that the pH of *Synechococcus* cultures increased when grown in a non-buffered medium (Martinho de Brito et al., 2022). In these growth
86 conditions, the production of EPS was enhanced compared to growth in a buffered medium. Furthermore, the EPS from cells grown in non-buffered conditions
87 contained more negatively-charged functional groups that impacted the properties of the carbonate minerals that precipitated. The current study further investigates
88 the properties of EPS produced during different growth phases of *Synechococcus* spp. Over an extended incubation time (mimicking a prolonged natural bloom). We
89 aim to better understand the role of cyanobacterial blooms in carbonate precipitation through EPS production and develop a conceptual model of picoplankton-
90 mediated organomineralization to explain the biological origin of whiting events.

91 2. Materials and Methods

92 2.1 *Synechococcus* PCC7942 strain and culture growth conditions

93 *Synechococcus* PCC7942 was obtained from the Centre de Ressources Biologiques de l'Institut Pasteur (Paris). Cultures were grown in a one-third-strength, non-
94 buffered liquid BG-11 medium (Allen, 1968; Rippka et al., 1979). The medium consists of (per liter): 1.5 g of NaNO₃; 0.04 g of K₂HPO₄·2H₂O; 0.075 g of MgSO₄·7H₂O;
95 0.036 g of CaCl₂·2H₂O; 6 mg of citric acid combined with 6 mg of ferric citrate; 0.001 g of Na₂EDTA·2H₂O and 0.02 g of Na₂CO₃. Trace metal solutions contained
96 (per liter) 2.86 mg of H₃BO₃; 1.81 mg of MnCl₂·4H₂O; 0.222 mg of ZnSO₄·7H₂O; 0.39 mg of Na₂MoO₄·2H₂O; 0.079 mg of CuSO₄·5H₂O and 0.0494 mg of

97 Co(NO₃)₂·6H₂O. Cultures were incubated at room temperature (21°C±2), in a light/dark cycle of 12h/12h under 36.8 μE m⁻² s⁻¹ of photon irradiance while shaken at
98 200 rpm in a Cimarec i Multipoint Stirrer, 6 Position, 2000 rpm, 3L per Multipoint, 100-240 VAC rotary shaker.

99 **2.2 Experimental design of *Synechococcus*-bloom formation**

100 Two independent growth experiments were performed in 1L glass serum bottles containing 800 mL of 1/3 BG-11 medium adjusted to pH 7.5, sealed with silicone caps
101 to allow gas exchange. Cells used for the inoculum (pH = 9.2) were pre-cultured in a full-strength BG-11. Immediately after inoculation (30 mL/bottle), the pH
102 increased to approximately 8.2.

103 **2.2.1 Experiment I**

104 In the first growth experiment, six bottles were inoculated with *Synechococcus* PCC7942. Cell growth and EPS production were examined. Optical density (OD_{750nm}),
105 pH and cell counts were monitored weekly (2-3 times by week). EPS was extracted on days 14, 28 and 56 of cultivation (two bottles were harvested at each sampling
106 time).

107 **2.2.2 Experiment II**

108 The second growth experiment was performed in quadruplicate. Chlorophyll *a* (Chl*a*), extracellular carbonic anhydrase activity (eCA), nutrients (NO₃⁻ and PO₄³⁻) and
109 calcium concentration were analysed at 0, 14, 28 and 56 days of cultivation. pH values, OD and cell counts were also assessed at longer intervals (once per week) than
110 in Experiment I.

111 **2.3 Growth assessment**

112 **2.3.1 pH values, optical density (OD) and cell counts**

113 The pH value was measured about 3-4 h after the light cycle started with a CRISON GLP 21 pH meter (Crison Instruments SA, Alella, Spain). Cell growth was
114 monitored through cell counts and OD₇₅₀ measurements. Cell counts were performed using a counting chamber (Neubauer, Mariangela, Germany) by randomly
115 selecting five fields of view and counting approximately 100-200 cells. The OD at 750 nm of a 1-ml sample of the culture was measured in a Bio-Rad SmartSpec Plus
116 Spectrophotometer (Bio-Rad, Hercules, CA, USA).

117 **2.3.2 Chlorophyll-a extraction**

118 Chl*a* was extracted from 2 ml culture aliquots using a methanol extraction method (Stal et al., 1984). Following the extraction in the dark at 4 °C, samples were
119 centrifuged. The Chl*a* absorbance was measured in the supernatant at 665 nm using a Bio-Rad SmartSpec Plus Spectrophotometer (Bio-Rad, Hercules, CA, USA).

120 **2.3.3 Extracellular carbonic anhydrase activity**

121 The extracellular carbonic anhydrase (eCA) activity was measured using a BioVision Carbonic Anhydrase Activity Assay Kit Kit (BioVision, Ref. K472-100, Abcam,
122 Waltham, MA, USA) according to the manufacturer's specifications. Aliquots of ~ 5 ml were analysed immediately after the collection. To avoid cell lysis and
123 intracellular CA contamination, samples were not centrifuged. The cells were separated from the supernatant by using a 1 mL syringe and a 0.20 μm NALGENE®
124 syringe filter. The absorbance was measured in a Bio-Rad Model 680 Microplate Reader at 405 nm.

125 **2.3.4 Nitrogen, phosphorus and calcium measurements**

126 Phosphate, nitrate and calcium concentrations were determined in the growth medium at 0, 14, 28 and 56 days of cultivation. Cells were removed by centrifugation
127 and filtration through a 0.20 μm Millipore filter under a mild vacuum. The samples were stored at 4°C in the dark until measured by ion chromatography. Analyses
128 were realized within the PEA²t technical platform of the Chrono-Environment Laboratory UMR6249 (Université de Franche-Comté, Besançon, France) and the Ca²⁺
129 concentration was determined by ICP-AES (dual axial and radial view iCAP Pro XP model with fast loop, Thermofisher Scientific, Courtaboeuf, France) available at
130 the University of Franche-Comté, Besançon, France.

131 **2.4 EPS extraction and purification**

132 EPS were extracted from the *Synechococcus* cultures as previously described by Martinho de Brito et al. (2022). EPS were harvested after 14, 28 and 56 days of
133 cultivation. Cyanobacterial cells were inspected by microscopy to ensure that no cell lysis had occurred during the extraction process. The pure EPS fractions were
134 obtained by ultrafiltration (>10 kDa = retentate) for volume reduction and the weight of the material was determined following by dialysis (using a 1 kDa Membrane)
135 lyophilization on a high-precision analytical balance (Quintix 35-1S, Sartorius, Gottingen, Germany).

136 **2.5 EPS characterization**

137 **2.5.1 Fourier Transform-Infrared Spectroscopy**

138 FT-IR spectra were obtained from freeze-dried EPS on an FT-IR Bruker Alpha spectrometer (Bruker Optics SARL, Marne la Vallée, France) fitted with an Attenuated
139 Total Reflectance (ATR) ALPHA-P device equipped with a mono-reflection diamond crystal. A total of 24 scans were performed on each sample at a spectral
140 resolution of 4 cm⁻¹ in the 4000–375 cm⁻¹ wavenumber range. The qualitative assignment of absorption bands was performed by comparison with spectra available in
141 the literature (Coates, 2000).

142 **2.5.2 Protein, sugar and glycosaminoglycan [quantification]**

143 The total protein content of EPS was determined using the Bicinchoninic acid assay (Pierce® BCA Protein Assay Kit) and bovine serum albumin as the standard. The
144 total sugar content was determined by a modified phenol-sulfuric acid method (Dubois et al., 1956) and xanthan and dextran were used as standards (Sigma-Aldrich,
145 St. Louis, MO, USA). The total glycosaminoglycan (GAGs) content was quantified using the Blyscan Assay according to the manufacturer's protocol (Blyscan Kit
146 B1000, Biocolor Ltd., Antrim, UK) with chondroitin sulphate as the standard. All assays were carried out in duplicated EPS samples.

147 2.5.3 Visualization of polyanionic macromolecules on Alcian Blue stained gels

148 Sodium Dodecyl Sulfate-Polyacrylamide Gel Electrophoresis (SDS-PAGE) followed by Alcian Blue staining (Wall and Gyi, 1988) were used to separate and to stain
149 negatively charged macromolecules (10- > 170 kDa), respectively. Alcian Blue is a dye that specifically binds to glycoconjugates with an acidic character (*e.g.*,
150 containing carboxylated or sulfated functional groups). Samples were analysed on one-dimensional precast gradient protein gels (TGX Gel 4-15%, 90 mm x 70 mm)
151 on a Mini-Protean 3 cell (Bio-Rad, Hercules, CA, USA), according to the method previously described by Martinho de Brito et al. (Martinho de Brito et al., 2022).
152 Prior to migration, samples were heat-denatured in standard 2x Laemmli sample buffer (5 min., 99°C, ref. 1610737, Bio-Rad). A pre-stained protein ladder
153 (Euromedex, #06P-0111; MW: 10 kDa to > 170 kDa) was used as a reference.

154 2.5.4 Inhibitory effect of EPS using pH-drift assay

155 The capacity of negatively charged functional groups in EPS to inhibit the *in vitro* precipitation of calcium carbonate was tested with the pH-drift assay (Wheeler et
156 al., 1981; Marin et al., 2000; Kawaguchi and Decho, 2002). This assay was performed as previously described by Martinho de Brito et al. (2022). Briefly, the pH was
157 recorded by a pH meter (Laboratory Research Grade Benchtop pH/mV Meter with 0.001 pH Resolution-HI5221) connected to a PC via a USB cable. Data were
158 recorded by the HANNA HI92000 software. The pH was measured every two seconds for ~15 min. The shape of the curve (after reaching its maximum, about one
159 minute after T₀) reflects directly the inhibitory capacity of the tested EPS: a fast decrease in pH (decreasing exponential) indicates ongoing precipitation i.e. the
160 absence of inhibition. A delayed decrease in pH, resulting in a plateau around pH 8, indicates an inhibitory effect, proportional to the length of the plateau. Between
161 each experiment, the electrode was refreshed with dilute acid and blank tests (without EPS) were performed.

164 2.6 Interaction of EPS with the *in vitro* precipitation of CaCO₃

165 The potential of the EPS matrix to interact with the precipitation of calcium carbonate was tested via the diffusion method in the presence of a closed ammonia-CO₂
166 saturated atmosphere (Albeck et al., 1993). 200 µL of the mixture containing pre-filtered (0.22 µm) CaCl₂ solution (10 mM) and EPS at increasing concentrations (3,
167 18, and 36 µg.mL⁻¹) were incubated in duplicate in 16-well plates (Lab-Tek, Nunc/Thermo Scientific, Rochester, NY, USA). The EPS concentrations were selected
168 to match the EPS yields at the extraction times (14, 28 and 56 days of cultivation). The plastic covers of the well plates were perforated to allow the reaction between
169 CaCl₂ solutions containing EPS and ammonium bicarbonate. The well plates were placed in a desiccator that was incubated at 4°C in the dark for 72 hrs. At the
170 completion of the incubation period, the pH value was measured in each well, the overlying solutions were carefully removed to dryness and CaCO₃ crystals analysed.
171 Blank experiments were performed without any EPS. The experiment was carried out in duplicates.

172 2.6.1 Morphology and mineralogy of the crystals

173 The 16-well plates containing crystals were used in two manners: first, the morphology of the CaCO₃ crystals was checked with a tabletop scanning electron microscope
174 (Hitachi TM 1000, Ibariki, Japan) in back-scattered electron mode. To this end, the glass plate base was unsealed from its plastic well part and directly observed
175 without carbon or gold sputtering. Secondly, the polymorph of the calcium carbonate minerals was determined by FT-IR spectroscopy using an FT-IR Bruker Alpha
176 (Bruker Optics, SARL, Champs-sur-Marne, France). Mineral phases were determined by comparison of the spectra with the reference spectra available in the RRUFF
177 Project database (<https://rruff.info>, accessed on January 1st, 2022).

178 2.6.2 Crystal counts and size distribution

179 CaCO₃ crystals were counted directly in the 16-well plates using an inverted microscope (Nachet, Paris, France) equipped with Mosaic 2.2.1 image analysis software.
180 Images were processed to obtain crystal sizes (average width and length of size classes < 50 µm and > 50 µm) and the total count of crystals in each well. A total of
181 ten fields of view (10 squares) accounting for 15.5 mm² were analysed. The results are reported as the mean ± standard deviation.

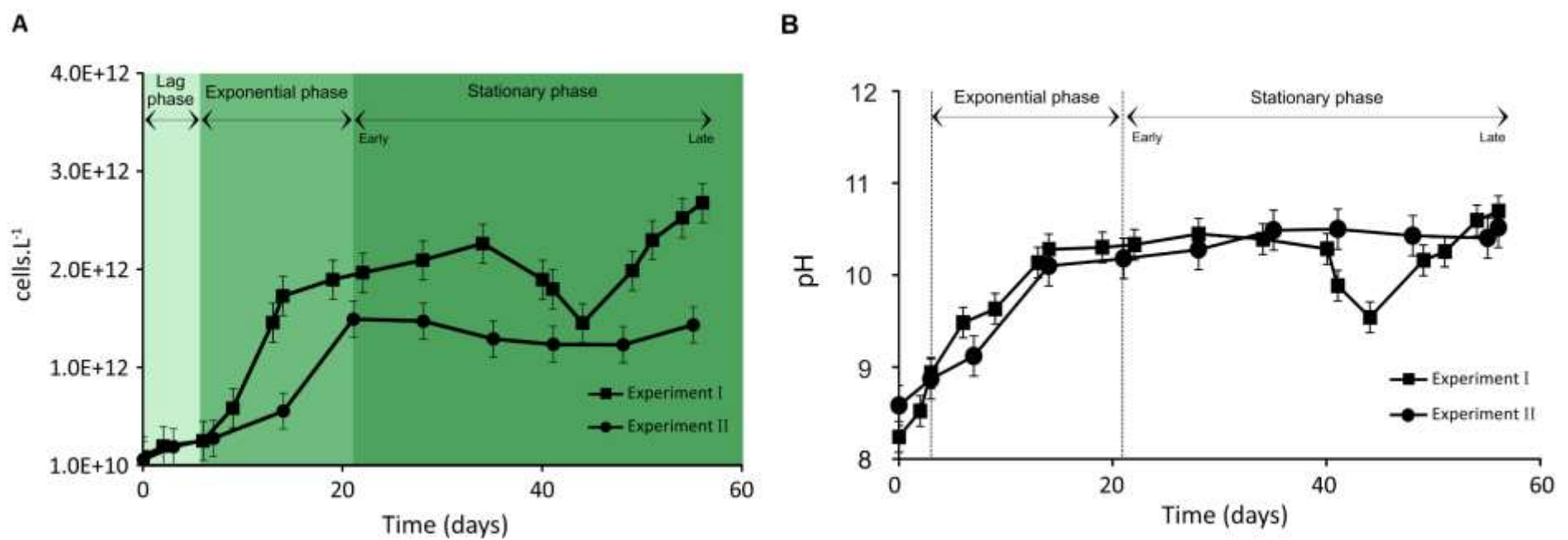
182 2.7 Statistical analysis

183 All the data concerning *Synechococcus* growth and EPS production are representative of two independent experiments with two technical replicates (four replicates
184 for EPS extracted at 56 days of culture). The results are reported as the mean ± standard error of the mean. Statistical significance was assessed by performing single-
185 factor ANOVA tests; p-values < 0.05 were statistically different.

186 3. Results

187 3.1 Trends in *Synechococcus* PCC7942 growth experiments and pH evolution

188 Cell density and pH values increased over the *Synechococcus* cultivation period (Figure 1A and 1B). The growth of *Synechococcus* cells showed a typical pattern
189 including a brief lag phase (~6-7 days) followed by a 7-day (experiment I) and 14-day (experiment II) exponential phase and finally a stationary phase. The stationary
190 phase (early stationary phase) was reached after 14 and 21 days of growth in experiment I and II, respectively, and lasted until day 56 of cultivation in both experiments
191 (late stationary phase) (Figure 1A). Growth experiments I and II started with a similar cell density of approximately 10¹⁰ cells.L⁻¹ and demonstrated reproducible
192 growth patterns (p-value = 0.91). At the time of inoculation, cell density was 9.5 × 10¹⁰ in experiment I and 7.1 × 10¹⁰ cells.L⁻¹ in experiment II (Figure 1A).
193 *Synechococcus* grew exponentially until reaching a maximum of 1.7 × 10¹² in experiment I at 14-day of growth and 1.5 × 10¹² cells.L⁻¹ after 21 days of growth in
194 experiment II. At the end of the exponential growth phase, the cell numbers levelled off and achieved a stable growth stage (stationary phase). Typical evolutions of
195 pH values in culture media during the *Synechococcus* growth experiments are presented in Figure 1B. As a general trend, pH is linked to the photosynthetic activity
196 of cyanobacteria. The pH levels rose rapidly during the exponential phase in both experiments, reaching around 10, and stayed steady during the stationary phase.
197 While experiment I experienced significant pH fluctuations during the latter part of the stationary phase, overall, the pH evolution trends for both experiments are
198 comparable (p-value = 0.91; Figure 1B). The p-values for pH and cell numbers showed that the two independent growth experiments are not significantly different.



199
200 **Figure 1.** Evolution of biomass of *Synechococcus* PCC 7942 culture (A) and pH evolution (B) during exponential, early and late stationary phases. The vertical dotted lines (B)
201 represent the stage transition between lag, exponential and stationary phases. Each value is the mean \pm SD of all replicate values.

202 3.2 Extracellular carbonic anhydrase

203 The activity of extracellular carbonic anhydrase (eCA) in solution changed slightly over the growth experiment (Figure 1S). The highest eCA activity (~1600) was
204 detected after 14 days of culture, during the exponential phase. The lowest activity was measured after 56 days of growth, in the late stationary phase.

205 3.3 Nutrient concentrations during growth

206 High nitrate concentrations supported exponential growth and high cell density (Table 1). The results show that a major decrease in nitrate and phosphate concentrations
207 occurred during the exponential growth phase and remained slowed down progressively over the stationary phase. At the end of the stationary phase, the phosphate
208 concentration had decreased to approximately 30% of its initial level. On the other hand, the nitrate concentration was still high, with approximately 67% of its initial
209 concentration remaining. Ammonium concentration was below the limit of detection ($2.2 \mu\text{M}$). Calcium concentrations decreased gradually and accounted for the
210 total calcium concentration of 81% in the late stationary phase. Other medium constituents should be present in excess and were thus not measured.

211
212 **Table 1.** Concentrations of NO_3^- , PO_4^{3-} and Ca^{2+} (μM) in the culture medium before inoculation (initial concentrations in the medium) and during exponential, early and late stationary
213 of *Synechococcus* growth phases are given as mean concentrations of four replicates (n=4).

Major anions and cations (μM)	Initial concentrations in the medium	<i>Synechococcus</i> growth phases		
		Exponential	Early stationary	Late stationary
NO_3^-	<u>7082\pm58.7</u>	<u>5731\pm328.9</u>	<u>5544\pm57.9</u>	<u>4716\pm250.1</u>
PO_4^{3-}	<u>68\pm0.6</u>	<u>39\pm4.7</u>	<u>41\pm2.2</u>	<u>21\pm6.7</u>
Ca^{2+}	<u>102\pm0.5</u>	<u>91\pm2.1</u>	<u>88\pm1.7</u>	<u>83\pm4.8</u>

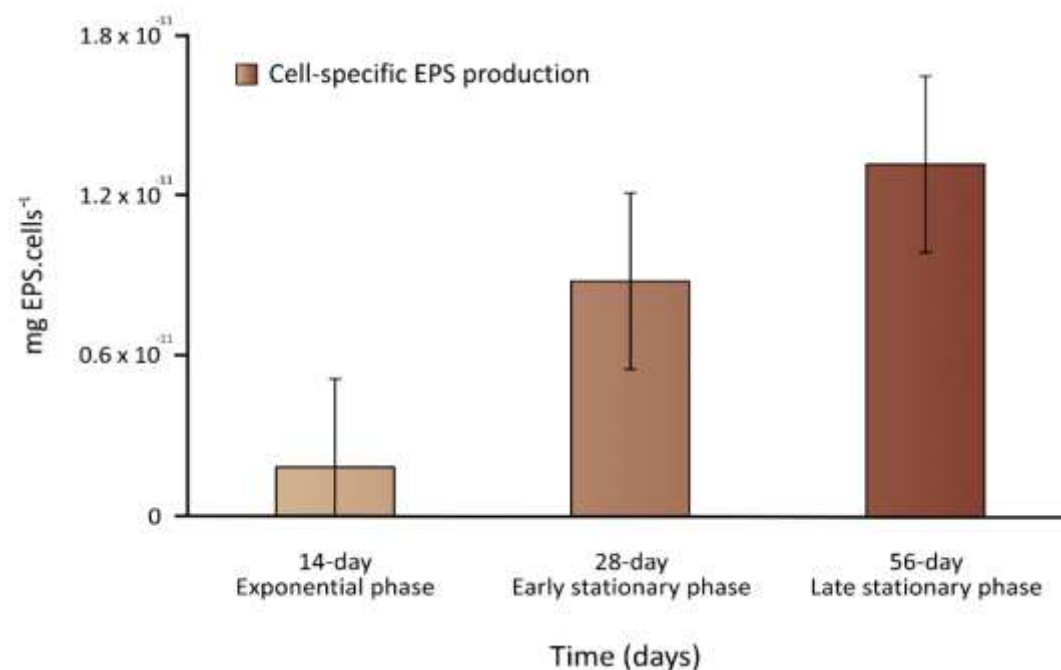
214 215 3.3 Abundance of EPS

216 The recovery yields of the EPS produced (mean \pm SD) resulting from the applied extraction method are listed in Table 2. The EPS yields varied from 2.9 ± 0.5 to
217 $18.6\pm 2.1 \text{ mg.L}^{-1}$ during exponential and early stationary phases and reached the highest yield of $35.4\pm 4.2 \text{ mg.L}^{-1}$ at 56 days of culture, in the late stationary phase
218 (Table 2). When the values were normalized per cell yield, results showed that the EPS concentration increased significantly between the exponential and late stationary
219 phases (p-value < 0.05) (Figure 2). *Synechococcus* continuously produced EPS during the 56-day experiment. In the first 14 days of growth, cells grew exponentially
220 and EPS production was deficient. Between exponential and early stationary phases, EPS production increased by a factor of five to seven, reaching a maximum in
221 the late stationary phase, after the 56-day growth experiment.

222
223 **Table 2.** Cell yield, total EPS production and cell-specific EPS production in *Synechococcus* PCC7942 cultures during exponential, early and late stationary growth phases. Data
224 represent the means of two independent experiments.

	Time of harvest (growth phase)		
	Exponential	Early stationary	Late stationary
Cell yield (cells.L ⁻¹)	$(161.6\pm 21.6)10^{10}$	$(211.2\pm 6.0)10^{10}$	$(268.8\pm 14.4)10^{10}$
EPS yield (mg.L ⁻¹)	2.9 ± 0.5	18.6 ± 2.1	35.4 ± 4.2
Cell-specific EPS production (mg. cells ⁻¹)	$(1.9\pm 0.6)10^{-12}$	$(8.8\pm 0.8)10^{-12}$	$(13.1\pm 0.9)10^{-12}$

225
226



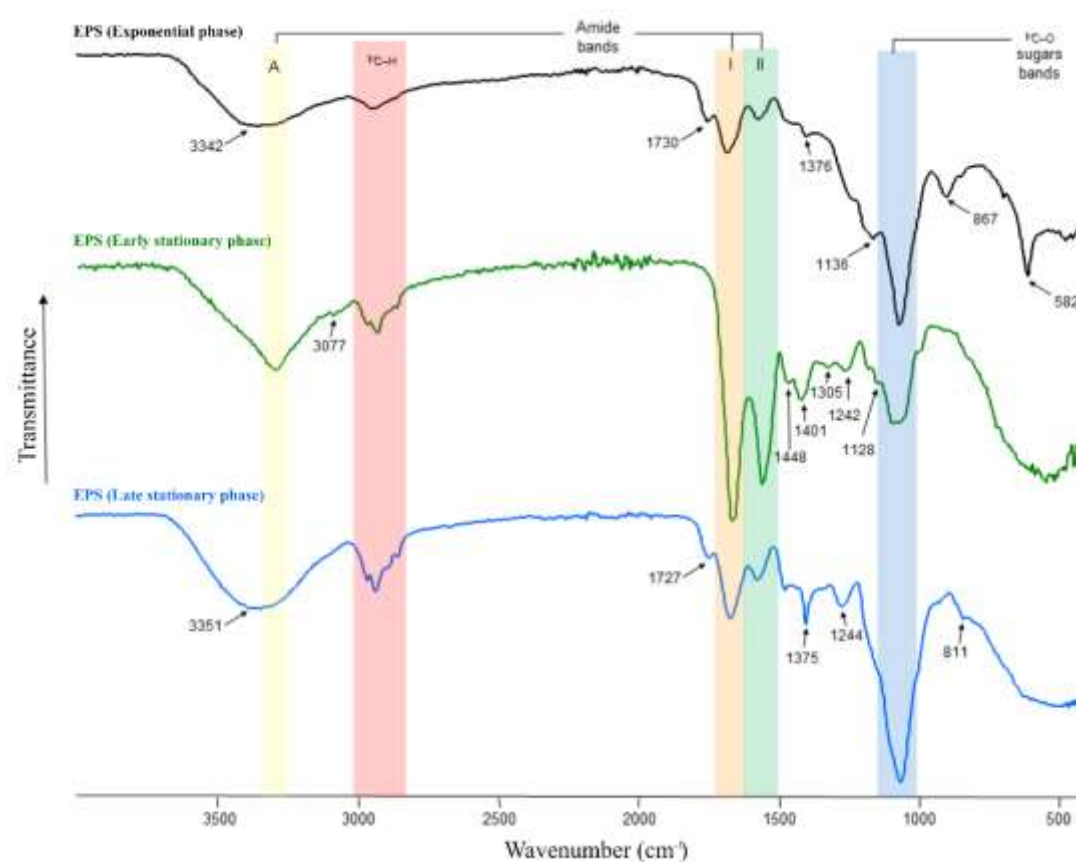
227
228

229 **Figure 2.** Cell-specific EPS production during the exponential, early and late stationary phases. MEAN±SD replicates from (n=2).

230 3.4 Chemical properties of EPS

231 3.4.1 FT-IR spectroscopy of EPS

232 FT-IR spectroscopy was used to check the overall EPS properties and composition. The IR spectra of EPS harvested during the exponential, early and late stationary
233 phases of the growth experiment are depicted in Figure 3. The three spectra show strong similarities, exhibiting characteristic absorption bands for polysaccharides
234 and protein moieties (highlighted in Figure 3 by vertical-coloured areas). However, differences in sample composition were also revealed by the presence of additional
235 absorptions indicated by arrows in Figure 3. Interestingly, the spectrum of the exponential phase EPS exhibits a strong band, isolated at 582 cm⁻¹, which according to
236 the literature on EPS could be assigned to a C–X stretch of alkyl halides (Kavita et al., 2011). Bands at 811–868 cm⁻¹, most likely representing the glycosidic linkage
237 between sugar monomers, were only present in EPS extracts in the early and late stationary phases. Bands at 1039 – 1128 cm⁻¹ (C–O and C–O–C stretching vibrations)
238 could be assigned to polysaccharides and polysaccharide-like structures (Wang et al., 2012) and were observed in all EPS samples (Figure 3, blue area). In contrast,
239 the small shoulders observed in the early and late stationary phase EPS, at ~1242 and 1244 cm⁻¹ correspond to sulfate groups (νS=O stretching vibrations). Low-
240 intensity bands observed in the range of 1370–1450 cm⁻¹ are assigned to CH₃ and CH₂ deformations (bends) of proteins (Kansiz et al., 1999). These absorption bands
241 were more evident in EPS obtained during the early stationary phase. The bands present in the range of 1660 and 1540 cm⁻¹ are attributed to C=O and C–N stretching
242 vibrations and are characteristic of Amide I and II functions (Figure 3, orange and green areas, respectively), which are typically associated with proteins (Coates,
243 2000). Spectra of the early stationary phase EPS showed higher peaks of protein than those observed in EPS from exponential and late stationary phases. The medium
244 bands at 1730 and 1727 cm⁻¹, present in samples extracted from exponential and late stationary phases, can be attributed to C=O stretching vibrations resulting from
245 lipids and fatty acids (Kansiz et al., 1999). Absorptions in the range of 2960–2850 cm⁻¹ corresponding to C–H stretching vibrations of aliphatic hydrocarbons and
246 possibly indicative of long-chain polymers (e.g., sugars or proteins), were observable in all EPS extracts. The amide A band (3345 cm⁻¹), characteristic of the N–H
247 vibration of peptide groups in proteins, is present in all spectra (Figure 3, yellow area), but is particularly visible on the early stationary phase EPS spectrum. In the
248 samples at 14 and 56 days of growth, this band is included in shoulders due to the presence of OH absorptions centred at 3342 and 3351 cm⁻¹, respectively. The list
249 of band assignments is summarized in supplementary material (Table 1S).



250

251 **Figure 3.** FT-IR spectra of EPS produced during the exponential (black line), early (green line) and late (blue line) stationary phases. Amide A absorbs in the range of 3342–3351
252 cm⁻¹ (yellow area), amides I-II at 1542–1650 cm⁻¹ (orange and green areas), sulfate groups at ~1242–1244 cm⁻¹, polysaccharides at ~1040–1070 cm⁻¹ (blue area), and the β-glycosidic
253 linkages are visible as a shoulder at ~867cm⁻¹.

254 3.4.2 Protein, sugar and glycosaminoglycan (GAGs) contents

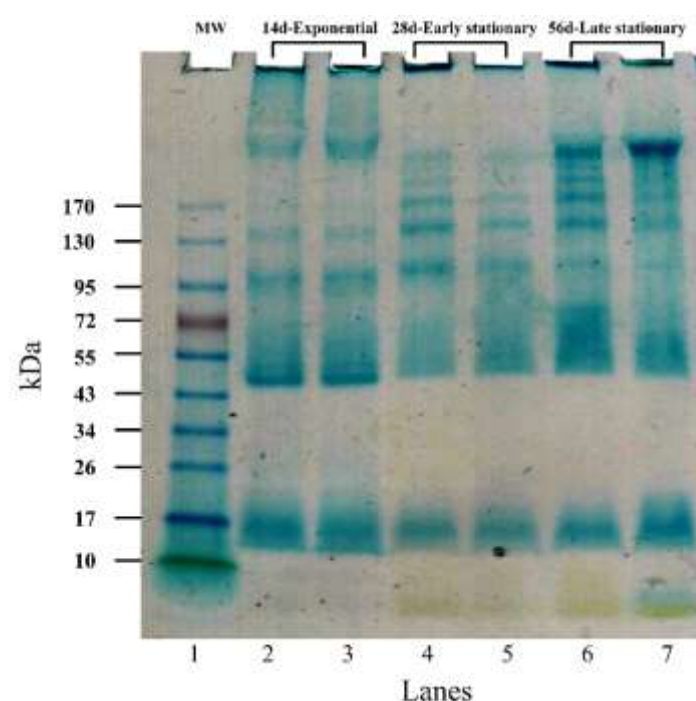
255 The EPS produced during the exponential growth phase revealed the lowest concentration of protein ($79 \pm 9 \mu\text{g} \cdot \text{mg}^{-1}$ EPS) (Table 3). The highest protein concentration
 256 was measured in EPS produced during the early stationary phase ($253 \pm 42 \mu\text{g} \cdot \text{mg}^{-1}$ EPS), whereas during the late stationary phase EPS, the protein concentration
 257 decreased by ~ two-fold. When accounting for the cell yield at times of EPS extraction, cells produced EPS with *ca* 11-15 times more protein in the stationary phase
 258 than in the exponential phase. The sugar content in the EPS harvested during the three different growth stages did not vary significantly. The EPS produced during the
 259 exponential phase contained a slightly higher sugar content ($584 \pm 9 \mu\text{g}$ of xanthan and $504 \pm 78 \mu\text{g}$ of dextran equivalents. mg^{-1} EPS) than that measured in EPS
 260 produced during the early and late stationary phases (1.8 times and 1.3 times lower, respectively). Our results show that, over the cultivation time, cells enhanced the
 261 production of larger amounts of glycosaminoglycans (GAGs) which can be associated with amino sugars and glycoproteins. The highest fraction of sulfated groups
 262 (GAGs) to total EPS ($217 \pm 143 \mu\text{g}$ GAGs. mg^{-1} EPS) was found in the late stationary phase EPS.

264 **Table 3.** Protein, sugar and glycosaminoglycan content of the harvested EPS at times 14, 28 and 56 days of *Synechococcus* PCC7942 culture. Values represent the average of four,
 265 three and two measurements of protein, sugar and GAGs, respectively, in two EPS replicated samples (n=2).

Components of EPS yield	Time of EPS harvesting (days/growth phase)		
	14 days Exponential	28 days Early stationary	56 days Late stationary
Protein ($\mu\text{g} \cdot \text{mg}^{-1}$ EPS)	79 ± 9	253 ± 42	128 ± 13
Cell-specific protein production (μg protein. cell^{-1})	$(1.5 \pm 0.6) \times 10^{-10}$	$(2.2 \pm 0.1) \times 10^{-9}$	$(1.7 \pm 0.0) \times 10^{-9}$
Sugar (μg xanthan equivalents. mg^{-1} EPS)	584 ± 95	326 ± 26	434 ± 11
Cell-specific sugar production (μg xanthan equivalent. cell^{-1})	$(1.0 \pm 0.2) \times 10^{-9}$	$(2.8 \pm 0.1) \times 10^{-9}$	$(5.7 \pm 0.2) \times 10^{-9}$
Sugar (μg dextran equivalents. mg^{-1} EPS)	504 ± 78	292 ± 22	381 ± 90
Cell-specific sugar production (μg dextran equivalent. cell^{-1})	$(8.9 \pm 1.4) \times 10^{-10}$	$(2.6 \pm 0.1) \times 10^{-9}$	$(5.0 \pm 0.2) \times 10^{-9}$
Glycosaminoglycans (μg GAGs. mg^{-1} EPS)	4 ± 0	31 ± 13	217 ± 143
Cell-specific GAGs production (μg GAGs. cell^{-1})	$(5.5 \pm 5.5) \times 10^{-12}$	$(2.6 \pm 0.8) \times 10^{-10}$	$(3.0 \pm 2.0) \times 10^{-9}$
GAGs/Sugar (xanthan) ratio	0.01 ± 00	0.09 ± 00	0.51 ± 0.3
GAGs/Sugar (xanthan) ratio	0.01 ± 00	0.10 ± 00	0.58 ± 0.4

267 3.4.3 SDS-PAGE

268 The results of gel electrophoresis after the migration of exponential, early and late stationary phase EPS samples are illustrated in Figure 4. Replicates showed similar
 269 band patterns that are distributed between 10 and > 170 kDa. A sharp greenish band in the migration front is strongly stained in late stationary phase EPS (Figure 4)
 270 and may correspond to chlorophyll. A less pronounced smear is visible in extracts obtained from the early stationary phase (Lanes 4 and 5). Bands of < 10 kDa were
 271 not detected in the EPS produced during the exponential phase (Lanes 2 and 3). A marked smear pattern is evidenced in all EPS extracted between 10-26 kDa: one
 272 prominent band was individualized at 17 kDa. A discrete blue smear (> 17-43 or 55 kDa) is evidenced in exponential phase EPS samples (Lanes 2 and 3) and is less
 273 obvious in EPS samples from the early and late stationary phase (lanes 4-5 and 6-7, respectively). No specific bands were individualized in the > 17-43 kDa molecular
 274 mass range, for the three growth phases. A band at about 45-47 kDa was strongly stained in exponential phase only. An area between 43 and 170 kDa was noted in all
 275 EPS extracts, accounting for 5-6 individualized bands that may correspond to the consecutive addition of an identical 'module', because the progression is logarithmic:
 276 is clearly seen in the early and late stationary phase lanes (lanes 4-7). The individualized bands were densely stained in EPS from the late stationary phase, including
 277 a smear at ~43-55 or 72 kDa (Lanes 6 and 7) and a prominent band at > 170 kDa (Lanes 6 and 7).

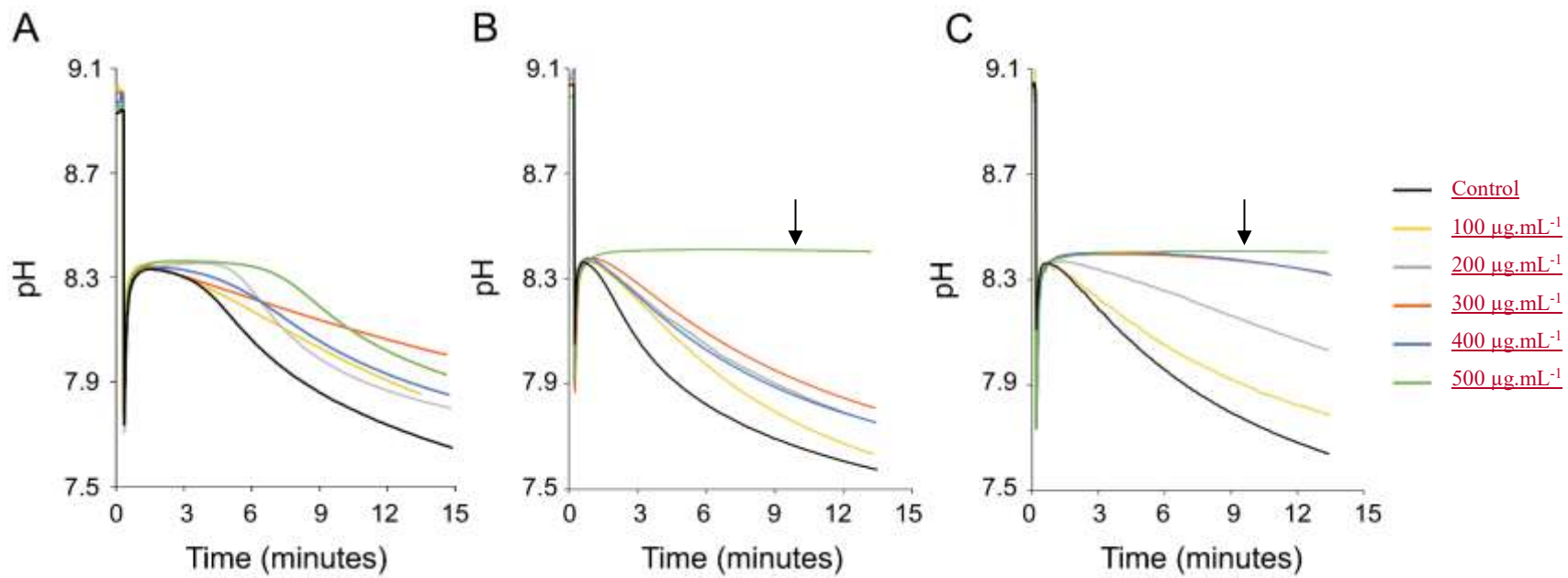


279 **Figure 4.** SDS-PAGE of EPS harvested during exponential (lanes 2-3), early (lanes 4-5) and late (lanes 6-7) stationary phases. Alcian blue staining was applied. The molecular ladder
 280 (MW) reference is shown in lane 1.

282 3.4.4 pH-drift assay

283 Recordings of the pH-drift assay are shown in Figure 5. The pH-drift assay determined the inhibitory effect of the EPS matrix (e.g., negatively charged functional
 284 groups) on the rate of CaCO_3 precipitation. Negatively charged groups of EPS can bind calcium ions from the solution and inhibit the nucleation of carbonates. When

285 CaCO₃ minerals start to nucleate, the pH of the solution decreases. Results show that the inhibitory effect was concentration-dependent and clear differences were
 286 visible between EPS extracted in the exponential (Figure 5A), early (Figure 5B) and late (Figure 5C) growth phases. EPS matrices from the stationary phase of culture
 287 growth (Figures 5B and 5C) exhibited a stronger inhibitory effect on CaCO₃ precipitation than the EPS extracted during the exponential phase (Figure 5A). Complete
 288 inhibition was only reached in EPS from early and late stationary phases when 50 µg of EPS.mL⁻¹ was tested. In this case, a drop in pH was not observed and nucleation
 289 of crystals did not occur (Figure 5B and 5C), which means that the inhibition was total. Conversely, the exponential phase EPS exhibited less inhibition of CaCO₃
 290 precipitation (Figure 5A). The shorter plateau shows that the mineral-binding capacity of the matrix delayed CaCO₃ precipitation but that consequently the pH dropped and
 291 visible precipitates formed, showing a less powerful inhibitory effect of the EPS compared to stationary phases EPS matrices.



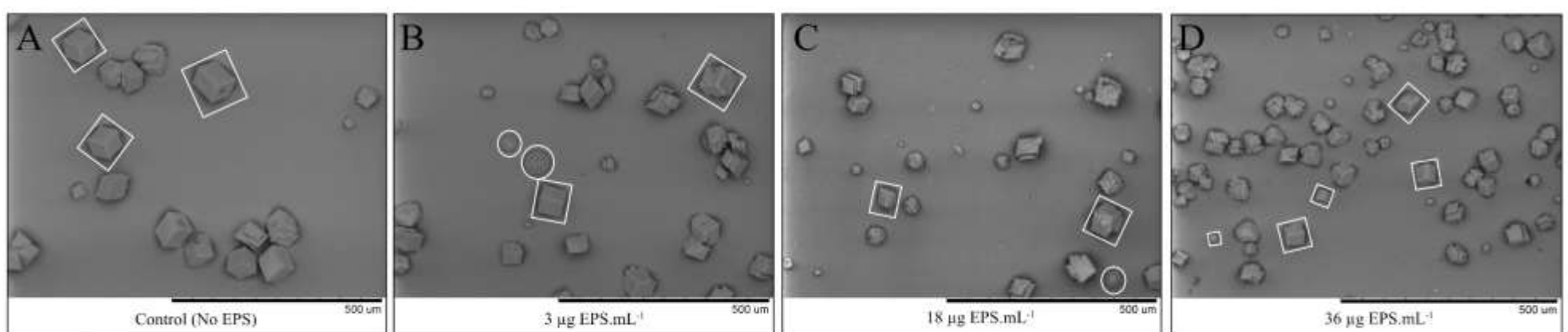
292
 293 **Figure 5.** *In vitro* inhibition of calcium carbonate precipitation by using EPS extracted during exponential (A), early (B) and late (C) stationary phases. Each panel shows the effect of
 294 six different EPS concentrations (0, 100, 200, 300, 400 and 500 µg EPS. mL⁻¹) on CaCO₃ precipitation, using the pH-drift assay method. The drop in pH indicates nucleation of CaCO₃
 295 (= precipitation) and a plateau indicates inhibition of precipitation. A larger plateau indicates a higher Ca-binding capacity of the matrix and thus stronger inhibition. Complete
 296 inhibition was observed when 50 µg of EPS solution from early and late stationary phases were used (e.g., see arrows). The results in each panel represent single experiments.
 297 Replication showed identical results (see Supplementary Figure 2S).
 298

299 3.5 Calcium carbonate crystallization in the presence of EPS

300 Forced CaCO₃ experiments were performed using a control solution (without EPS) and EPS solutions, at same pH, with concentrations of 3, 18 and 36 µg.mL⁻¹. Each
 301 concentration corresponds to the EPS yield at different growth stages: exponential phase (= 3 µgEPS.mL⁻¹), early (18 µgEPS.mL⁻¹) and late (36 µgEPS.mL⁻¹) stationary
 302 phases. The crystals formed in the various EPS solutions showed different morphological (Figure 6) and mineralogical (Figure 3S) features as well as distinct crystal
 303 sizes and distributions compared to those formed in control solution (Figure 7).

304 3.5.1 Mineral morphology

305 A preliminary light microscopic analysis was carried out in order to identify the most significant samples to analyse by SEM (Figure 6). The morphology of crystals
 306 precipitated in the negative controls was very homogeneous and predominantly composed of calcite rhombohedrons that sometimes formed polycrystalline aggregates
 307 of size > 50µm (Figure 6A). All control solutions tested for the various EPS harvested during exponential and stationary phases showed similar crystal characteristics.
 308 In the EPS solutions, CaCO₃ crystals showed both rhombohedral and spheroidal morphologies (Figure 6B-D). The morphology of crystals appears to change with
 309 increasing EPS concentrations. Spherical minerals formation was observed in the exponential phase-EPS solution (Figure 6B) and were less frequent in the EPS
 310 solution from early stationary phase (Figure 6C). In the late stationary phase-EPS solution, rhombohedrons represented the prevalent crystal morphology while
 311 spherical minerals were absent (Figure 6D).
 312



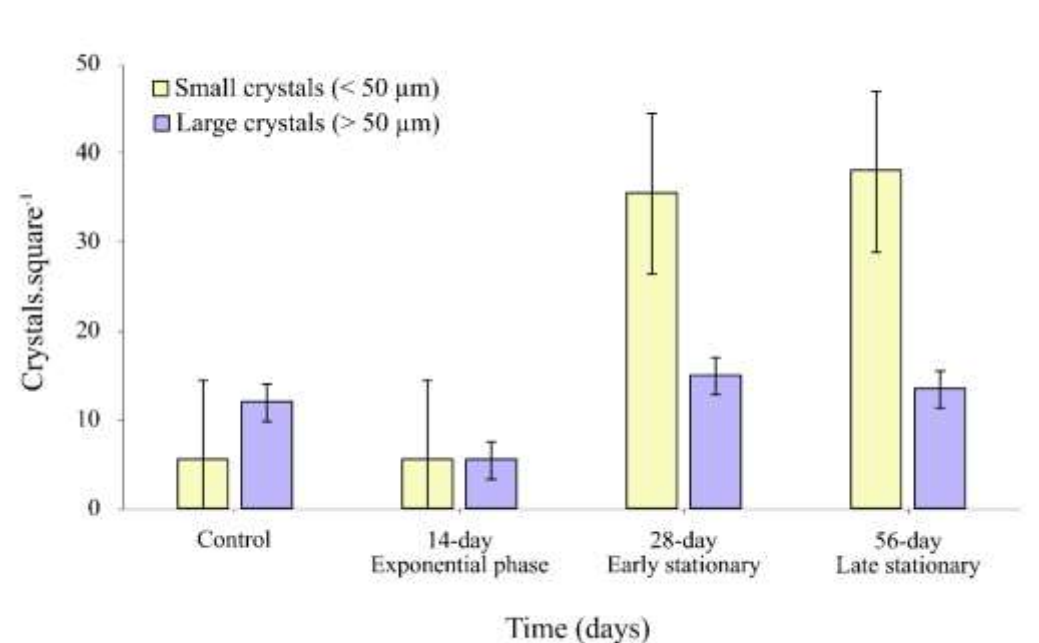
313
 314 **Figure 6.** *In vitro* forced CaCO₃ precipitation assay in (A) the absence of the EPS (control solution) and in the presence of EPS extracted during the (B) exponential, (C) early and (D)
 315 late stationary phases under increasing EPS concentrations of 3, 18 and 36 µg.mL⁻¹, respectively. The images show two different CaCO₃ morphologies: rhombohedral (white squares)
 316 and spheroidal (white circles), in some cases shown as polycrystalline crystals. The scale bar (black) at the bottom right of the images is 500 µm.

317 3.5.2 Crystal mineralogy

318 The crystals' mineralogy was assessed by FT-IR microscopy performed on selected individual crystals of $> 10 \mu\text{m}$ (Figure 3S). The results revealed that calcite was
319 the only CaCO_3 polymorph formed in the control solution. Calcite and vaterite formed in all EPS solutions tested. The FT-IR spectra revealed that all rhombohedrons
320 and polycrystalline aggregates with “sharp edges” represent calcite polymorphs. In contrast, spheroidal crystals revealed a vaterite signature (Figure 3S).

321 3.5.3 Crystal size and distribution

322 The results from image analysis showed that a larger quantity of crystals precipitated in the stationary phase (early and late) EPS solutions (Figure 7) and that major
323 differences were also observed in crystal size distribution (Figure 7). A comparison of the class of small crystal sizes ($< 50 \mu\text{m}$) with the large crystal size class
324 ($> 50 \mu\text{m}$) showed a clear trend of an increasing total number of small crystals in the stationary phase EPS solutions compared to those formed in the EPS solutions
325 from the exponential phase. The size reduction of the crystals at 18 and 36 mg/L (Figure 7, early and late stationary phases) suggests a partial inhibitory effect of the
326 EPS on the formation of calcium carbonate.



327
328 **Figure 7.** Total numbers of small ($< 50 \mu\text{m}$) and large ($> 50 \mu\text{m}$) crystal size classes of precipitated CaCO_3 in EPS solutions obtained from exponential and stationary phases, in EPS
329 concentrations of 3, 18 and $36 \mu\text{g.mL}^{-1}$, respectively.

330 4. Discussion

331 Our study demonstrates that the amount and properties of EPS change significantly ($p\text{-value} < 0.05$) at the three different stages of *Synechococcus* growth in an
332 artificial bloom experiment. Cells continuously produce EPS that increases in concentration and become more negatively charged in the stationary phase. We sampled
333 this EPS over the exponential, early and late stationary phases and studied its role in carbonate mineral precipitation. Based on this, a conceptual model was developed
334 to correlate the findings of this investigation with the potential EPS production of the naturally occurring picoplankton blooms and its possible involvement in whiting
335 events. Though natural blooms experience a variety of factors that are not represented in the experiments described in this paper, the first part of the discussion is
336 focussing only on the experimental data, whereas the interaction of these basic processes with other biotic and abiotic factors acting in the environment is discussed
337 afterwards.

338 4.1 Exponential growth phase

339 Macronutrients, such as nitrogen (N) and phosphorus (P) promote the initiation of cyanobacterial blooms (Reynolds and Walsby, 1975; Paerl, 2008; Xu et al., 2015).
340 In our growth experiment, the beginning of the exponential phase (and the persistence of bloom) (Figure 1A) was positively correlated with the high initial nutrient
341 concentration in the medium (Table 1). Environmental factors such as water temperature, light intensity, hydrodynamics and availability of dissolved inorganic carbon
342 (DIC) are also important determinants of cyanobacteria bloom development (Clark and Flynn, 2000; Dokulil and Teubner, 2000; Havens, 2008). Blooms can
343 dramatically alter the supply of inorganic carbon for photosynthesis, which causes the pH to increase (Ibelings and Maberly, 1998). In the early exponential phase of
344 our batch cultures, the high photosynthetic activity of cyanobacteria cultures resulted in fast pH increase thereby reducing the total inorganic carbon of the grown
345 medium. Light and CO_2 are the sources of energy and carbon for cyanobacteria, and are of critical importance for their growth (Takahashi et al., 2004). At pH 9
346 (Figure 1B), the concentration of CO_2 predicted is close to zero ($< 1 \mu\text{M}$) and the HCO_3^- concentration is $475 \mu\text{M}$ (PhreeqC data). A similar scenario was observed in
347 natural blooms occurrence: the population of cyanobacteria draws down the partial pressure of CO_2 ($p\text{CO}_2$) in the photic zone, increasing the surface water pH up to
348 9-10 (Ibelings and Maberly, 1998; Verspagen et al., 2014) and CO_2 concentration can become completely depleted or reach values close to zero (Maberly, 1996).
349 Under extreme conditions, the concentration of HCO_3^- can also become markedly reduced (Talling, 1976; Maberly, 1996). When the rate of photosynthesis is greater
350 than the combined rate of resupply of CO_2 from the atmosphere and DIC in the hypolimnion, deviation from the air equilibrium occurs, favouring CaCO_3 precipitation.
351 The pH of most aquatic systems ranges from 7.5-8.1 and keeps inorganic carbon primarily in the form of bicarbonate (O'Neil et al., 2012). In poorly buffered systems,
352 such as highly productive lakes, the pH and speciation of DIC experience large fluctuations which vary widely on a scale from daily (diel) to episodic, to seasonal
353 (Maberly, 1996) with diel variations as high as two pH units and $60 \mu\text{mol DIC.L}^{-1}$ (Maberly, 1996). Because CO_2 favors the C_3 photosynthesis (C_3 cycle operation of
354 Calvin-Beson cycle), the high pH of ~ 10 in our growth medium could be associated with carbon limitation (Ibelings and Maberly, 1998; Verspagen et al., 2014).
355

356 To alleviate CO₂ limitation, cyanobacteria have developed an efficient CO₂-concentrating mechanism (CCM) (Aizawa and Miyachi, 1986; Badger and Price, 1992;
357 Badger et al., 2002; Burnap et al., 2015) and can use bicarbonate as an inorganic carbon source for photosynthesis (Price et al., 1998; Giordano et al., 2005; Sandrini
358 et al., 2016). By activating CCM, cyanobacteria concentrate CO₂ by a factor of up to a thousand (Badger and Andrews, 1982; Badger et al., 2002; Price, 2011). CO₂-
359 deficient conditions experienced during the exponential phase of our growth experiment, coupled with the continuous cellular demand for inorganic carbon to support
360 photosynthetic carbon fixation likely led the cells to activate CCM. The predicted concentrations of CO₂ and HCO₃⁻ in the growth medium (PhreeqC data) in the early
361 and late exponential phase infer that *Synechococcus* cells actively transported across the membrane and accumulated DIC into the cell, where the HCO₃⁻ pool was
362 utilized to generate elevated CO₂ levels around Rubisco (Badger et al., 2002; Price et al., 2008). The CCM of cyanobacteria accomplishes very high carbon
363 concentrating factors ($C_{\text{external}} : C_{\text{internal}}$) at deficient specificity factors of RuBisCo (Tortell, 2000; Tortell et al., 2000). CCM involves bicarbonate transporters in the
364 cell membrane, intracellular (iCA) and extracellular (eCA) carbonic anhydrase enzymes and concentrated RuBisCO activity located in carboxysomes (Badger et al.,
365 2006; Price et al., 2008; Rae et al., 2013). CA converts HCO₃⁻ to CO₂ (Badger and Price, 1994), which increases the external pH in close proximity to the cells. In our
366 study, eCA activity was ~ 1.6-2.0 times higher during the exponential growth phase and reduced gradually through the stationary phase (Supplementary Figure 1S).
367 The strongly stained band only present in the exponential phase-EPS at around 45-47 kDa (Figure 4, lanes 2, 3) may be indicative of eCA, as reported by Kupriyanova
368 et al., 2018, but this requires further investigation. Another plausible explanation for the 45-47 kDa band could be the presence of chlorophyll f synthase, which
369 typically migrates at around 46 kDa (Shen et al., 2019). Similarly, Yang et al. (2023) measured the CA anhydrase in solution over a 30-day growth experiment with
370 *Synechococcus* PCC 7942 and reported an increase over the lag phase and large fluctuations over the exponential phase. During the stationary phase, CA did not vary
371 greatly but a minor decrease was recorded in the late stationary phase (Yang et al., 2023). In our study, the higher eCA activity recorded could explain the strongly
372 stained ~45-47-kDa band that was only identified in our SDS-PAGE gels of EPS produced during the exponential phase (Figure 4, lanes 2-3). The molecular weight
373 (MW) of this band is similar to a 42-43 kDa eCA previously identified by Kupriyanova et al. (2018) and discussed by Martinho de Brito et al. (2022). As explained
374 in the Results section 3.4.3, we cannot exclude that the band is chlorophyll f synthase, which seems to show up around 46 kDa. A more substantiated demonstration
375 of the identity of the SDS-PAGE band will require other approaches (beyond the scope of the present study), such as micro-sequencing of the purified 43 kDa band
376 or the use of a CA-specific antibody.

377

378 Active uptake of HCO₃⁻ and accumulation of Ci species requires the input of metabolic energy e.g., ATP (BCT1 HCO₃⁻ transporter), NADPH or reduced ferredoxin
379 (CO₂ uptake) or coupling to an electrochemical Na⁺ gradient (SbtA or BicA HCO₃⁻ transport) (Badger et al., 2002; Price et al., 2008). This energetic cost may therefore
380 reflect on the growth rates achieved. *Synechococcus* PCC 7942 grows at > 80% of its maximum growth rate when provided with HCO₃⁻ as its main inorganic carbon
381 source (Miller et al., 1984). During the exponential phase, the carbon production from photosynthesis is mainly allocated for biomass production, not for EPS synthesis.
382 During this phase (Figure 2 and Table 2), the small amount of EPS produced comprises a higher proportion of sugars and lower amounts of protein and GAG compared
383 to EPS produced during the stationary phase (Figure 3 and Table 3). Our study indicates that rather than proteins, sugars are the major component in all EPS extracts.
384 This finding is supported by the data obtained from FTIR analysis (Figure 3). The smaller amount of negatively charged groups of the EPS during the exponential
385 phase (Figure 4, lanes 2-3) compared to those of EPS from the early and late stationary phases (Figure 4, lanes 4-7) resulted in weak to moderate inhibitory capacity
386 (Figure 5A). The main phenomenon observed in the pH-drift assay (Figure 5) is the initial Ca binding to negatively charged groups in EPS prior to carbonate addition,
387 which initiates CaCO₃ precipitation. This results in a decrease of pH. The pH drift assay showed that EPS from exponential phase (Figure 5C) having a larger plateau,
388 and thus a lower a calcium binding capacity than the EPS from the stationary phase. This observation was further corroborated by the forced precipitation experiments,
389 which showed that EPS from the exponential phase induced small amount of mostly large-sized carbonate crystals (>50 μm), very similarly to the negative control
390 experiment (Figure 7) (Martinho de Brito et al., 2022). The high concentration of Ca²⁺ in the medium (83 μM) compared to the initial [Ca²⁺] at the beginning of the
391 experiment (103 μM), indicates that a small amount of calcium ions was bound to negatively charged functional groups of EPS (Table 1, see [Ca²⁺]).

392 In our batch experiment, cells continue to grow exponentially for ~20 days of cultivation. At this point, cultures reached the maximum cell density (Figure 1A) and
393 pH values ranged between 10-11 (Figure 1B). Based on our calculations, under these alkaline conditions, CO₂ was completely depleted (1.7×10^{-3} μM) in the growth
394 medium, whereas HCO₃⁻ was extremely low (~ 79 μM). Thus, the dominant inorganic carbon speciation was CO₃²⁻ (421 μM). Because cells cannot take up CO₃²⁻ and
395 HCO₃⁻ concentration seems to be insufficient to cover the carbon demands of cyanobacterial growth, we assume that this may have been the cause of cell numbers
396 starting to level off (Figure 1A, early stationary phase). Consequently, cultures entered a stationary state due to a lack of inorganic carbon availability required to
397 increase cell population (Miller et al., 1984; Mayo et al., 1989; Verspagen et al., 2014). The excess of nutrients measured in the medium in the late exponential phase
398 (Table 1) suggested that the specific growth rate was not limited by nutrient availability but by a rather low level of CO₂ carbon content.

399

400

401 4.2 Early stationary phase

402 Insufficient CO₂ availability is considered to be the external stress factor constraining the growth rate of cyanobacteria (Maberly, 1996; Hein, 1997; Ibelings and
403 Maberly, 1998) and low [HCO₃⁻] could sustain a constant population density for at least ~ 40 days (See Figure 1A, stationary phase). Our results suggest that at this
404 point, carbon fixation was allocated to EPS synthesis, not to biomass production (Miller et al., 1984). Increased EPS production is usually associated with external
405 stress factors (Rossi and De Philippis, 2015), including high pH conditions (Martinho de Brito et al., 2022). Moreover, metabolic stress may also alter the composition
406 of EPS (Babele et al., 2019; Martinho de Brito et al., 2022). In the present study, the negative functional group abundance increased, resulting in a higher acidity of
407 EPS (Figure 4, lanes 4-5) due to an increase in protein and sulfated glycan (GAG) (Table 3). In the pH conditions of the early stationary phase, all the functional
408 groups of the EPS matrix are deprotonated and are able to bind calcium ions (Figure 5B) (Dupraz and Visscher, 2005; Braissant et al., 2007; Dittrich and Sibling, 2010)
409 and bind calcium more efficiently nanometric nuclei in formation (if their formation is thermodynamically favoured). We suggest that the increased calcium-binding
410 capacity of the EPS probably accounts for lower the Ca²⁺ concentration measured in the medium (Table 2, see [Ca²⁺]). In our *in vitro* forced precipitation assay, we
411 measure the second effect, the inhibitory one (mineral-binding effect), which results in the production of small-sized calcium carbonate crystals (< 50 μm), in
412 comparison to what happens in the exponential phase (Figure 7).

413

414 4.3 Late stationary phase

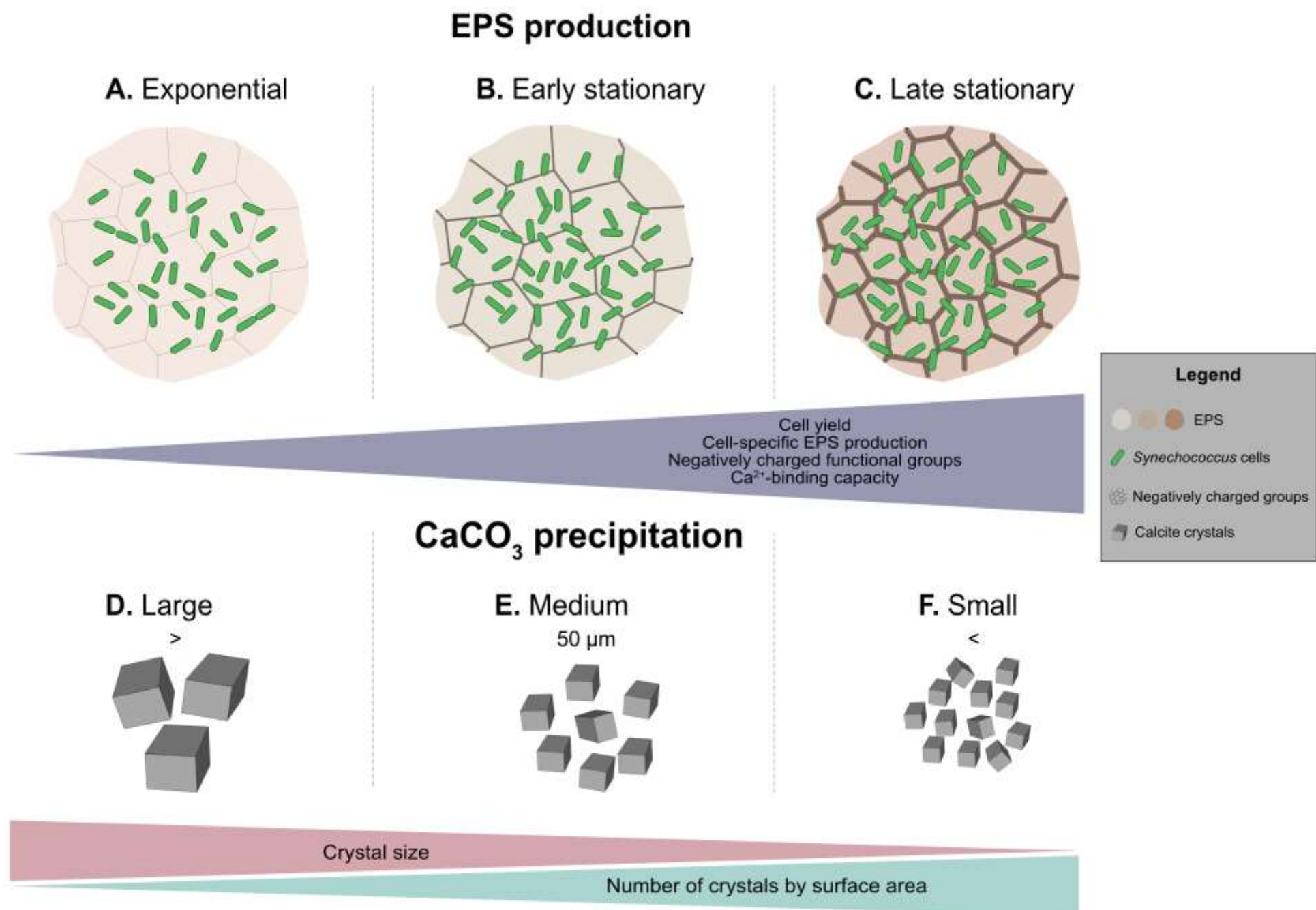
415 As mentioned above, we assume that the continuous increase in EPS production over the late stationary phase, including an overall augmentation of negatively charged
416 functional groups (Figure 4, lanes 6-7), including GAG content (Table 2), might be a specific response to a stress scenario. As expected, the present study shows that
417 the greater amount of negatively charged functional groups of EPS from the late stationary phase (Figure 4, lanes 6-7) resulted in a higher Ca-binding capacity than
418 exponential and early stationary phase-EPS (Figure 5C). Our forced precipitation experiments showed that minerals produced in the late stationary-EPS solutions are
419 smaller and more abundant than those formed in EPS solutions from the early stationary phase (Figure 7). Under natural conditions, when the Ca^{2+} supply is continuous,
420 the crystals may or may not continue to grow, depending on the physical space within the EPS matrix (Dupraz et al., 2009). Based on the high concentration of nitrate
421 ($4720 \mu\text{M}$) measured in the late stationary phase (Table 1), we assume that the abundance of this nutrient supported the persistence of the stationary phase, i.e., similar
422 to a prolonged bloom in natural conditions. The death phase was not observed in our 56-day-long experiment. Given that our cultures were continuously stirred, we
423 can assume that light was not limiting cyanobacterial growth. Furthermore, in natural blooms, the increase in population density may affect cells at greater depth
424 through self-shading by decreasing the light available for photosynthesis (Townsend et al., 1994). Yet, cyanobacteria (including *Synechococcus*) are known to be well-
425 adapted to low-light conditions (Campbell and Carpenter, 1986; Palenik, 2001; Callieri et al., 2011). Additionally, the presence of sulfated constituents on late
426 stationary phase-EPS contributes to a higher negative charge of the matrix and higher Ca-binding potential (Decho and Kawaguchi, 2003; Skoog et al., 2022), compared
427 to EPS extracted in the exponential phase which contained significantly lower GAG (Table 2). The present study shows that the greater amount of negatively charged
428 functional groups of EPS from the late stationary phase (Figure 4, lanes 6-7) resulted in a higher Ca-binding capacity than exponential and early stationary phase-EPS
429 (Figure 5C). Our forced precipitation experiments showed that minerals produced in the late stationary-EPS solutions are smaller and more abundant than those
430 formed in EPS solutions from the early stationary phase (Figure 7), suggesting an increased inhibitory ability of the late stationary-EPS.

432 4.4 Natural bloom and formation of whittings – Conceptual model

433 Our observations made during exponential and stationary phases can be applied to generate a conceptual model of EPS properties during a *Synechococcus* bloom
434 event (Figure 8A-C). The onset of a bloom starts with an increase in cell numbers, with high values in spring-summer (exceeding 10^5 - 10^7 cells.mL⁻¹) and lower values
435 in winter months ($< 10^5$ cells.mL⁻¹) in both marine (Agawin et al., 1998; Philips et al., 1999) and freshwater (Maeda et al., 1992; Tai and Palenik, 2009) environments.
436 This resembles the exponential growth phase in our study (Figure 1, exponential phase). We predict that during the initial phase of a natural bloom, there is little EPS
437 production: cells grow relatively quickly and the carbon fixed during photosynthesis is predominantly allocated to biomass production (Figure 8A). The fast growth
438 is followed by a phase during which cell numbers level off, typically due to stress conditions, which is represented by the early stationary phase in our study. Under
439 certain conditions, blooms can be sustained for weeks and possibly longer (Anderson et al., 2002; Havens, 2008; Zhao et al., 2013), similar to what we observed in
440 our growth experiments (Figure 1A, early stationary phase). The maintenance of a bloom requires continuous input of nutrients, which is also the case in our experiment
441 (Table 1) or in the case of natural systems, a turnover from lysing cells recycled by other microbes. During this phase, we did not observe a significant increase in cell
442 density but the production of EPS continued at a disproportionately high rate (Figure 8B-C). Our findings are in agreement with the lab studies using diatom cultures
443 which show that EPS production is low during exponential growth and increases in the stationary phase (Myklestad and Haug, 1972; Myklestad et al., 1989; Bhosle
444 et al., 1995). These authors reported that nutrient-deficient conditions enhanced the production of EPS over the growth phases. If carbon fixation continues and some
445 critically required nutrient is lacking from the growth medium, most likely the phototrophic organisms produce carbohydrate reservoirs (Ciebiada et al., 2020). These
446 include storage polymers like glycogen and the production of other carbohydrate-rich compounds, including EPS (De Philippis et al., 1996, 2001; Decho and Gutierrez,
447 2017). The decline of blooms in natural environments is typically associated with nutrient, low or high light intensity, grazing or viral infection. Under these stressful
448 conditions, an increase in EPS production by the phyto/picoplankton community may be expected.

450 *Synechococcus* spp. blooms can cause whiting events (Thompson, 2000), characterized by the presence of large amounts of CaCO_3 minerals in surface water. Various
451 mechanisms have been proposed for this phenomenon, including chemical and physical processes (Shinn and Steinen, 1989; Larson and Mylroie, 2014) as well as
452 biologically mediated precipitation (Thompson and Ferris, 1990; Robbins and Blackwelder, 1992; Stanton et al., 2021). However, no consensus has been reached on
453 the precise cause of these events. Carefully transporting the results from forced precipitation experiments to a whiting event, we suggest that early in the bloom (Figure
454 8A), relatively large CaCO_3 crystals form, provided sufficient Ca^{2+} is available (Figure 8D). As the bloom continues to grow, progressively the larger quantity of
455 negatively charged functional groups in the EPS provides more cation-binding sites and thus inhibits calcium carbonate precipitation largely. Depending on the three-
456 dimensional structure of the EPS and surface properties (Wang et al., 2012), nucleation may yield smaller CaCO_3 crystals (Figure 8). If this occurs, then the production
457 of a more negatively charged matrix (largely contributed by the enrichment in sulfated polysaccharides) may offer some selective advantage to the cyanobacteria
458 population, by inhibiting and/or delaying mineral precipitation and by reducing crystal size formed around the cells. This might result in slow sinking rates, extending
459 the residence time of the cyanobacterial community in the photic zone. If the bloom occurrence is short (e.g., similar to 14-28 days in our growth experiment), minerals
460 making up the whiting will be relatively larger. Consequently, the aggregates of cyanobacteria, EPS and CaCO_3 minerals may sink faster because mineral precipitation
461 in EPS increases the cyanobacterial-specific density several-fold. The *Synechococcus* specific density (ρ) is $1.040 \text{ g}\cdot\text{cm}^{-3}$ (Reynolds, 1987), near-neutrally buoyant,
462 whereas ρ_{calcite} is $2.710 \text{ g}\cdot\text{cm}^{-3}$ (Lange, 1999). The production of larger amounts of more negatively charged EPS may act as a protection mechanism against carbonate
463 formation in the vicinity of the cell wall (Martinez et al., 2010; Bundeleva et al., 2012), thus allowing the organisms to reside longer in the photic zone. Interestingly,
464 the production of EPS that contained sulfated groups among bacteria seems to be exclusive to cyanobacteria (Pereira et al., 2009; Maeda et al., 2021). Maeda et al.
465 (2021) reported that the cyanobacterium *Synechocystis* 6803 produced large amounts of GAG compounds during an experimental bloom formation. The authors
466 suggested that these constituents can be advantageous for the development of surface bloom as it may increase the buoyancy, permitting cells to migrate upward
467 rapidly when the water column is stable (Walsby et al., 1995). Thus, GAG production may be considered as an alternative for organisms that lack gas vesicles to
468 remain longer in the photic zone (Maeda et al., 2021). The negative charge of EPS produced containing high sulfated content also protects the community against viral
469 infection (Matsunaga et al., 1996). Therefore, the production of GAG by pelagic cyanobacteria contributes to stress tolerance and viral infectivity, helping in the
470 persistence of bloom. In our growth experiments, a decline in cell numbers was not observed, which would represent the end of the bloom. In the natural environment,
471 nutrient depletion, grazing or viral lysis/infection are the most likely causes of terminating a bloom (Gons et al., 2002). The cell lysis releases organic matter, which

472 supports the growth of heterotrophic bacteria (Kjelleberg et al., 1987; Hagström et al., 1988; Kieft et al., 2021). Photosynthetically derived organic carbon is one of the
 473 major carbon and energy sources for heterotrophic bacteria (Allgaier et al., 2008). These heterotrophs can degrade EPS and liberate bound Ca^{2+} (Visscher et al. 1998;
 474 Ionescu et al., 2015; Diaz et al., 2017). In addition, microbial respiration will produce $\text{HCO}_3^-/\text{CO}_2$, increasing the saturation index of CaCO_3 , and may enhance the
 475 whiting (Figure 8). Although our model is [somewhat] largely theoretical at this stage and explore the role of one picoplankton species, its merit is to focus on an
 476 overlooked actor of whiting events, the EPS. Furthermore, it provides a conceptual framework to work with, for designing novel experiments and measurements both
 477 in natural systems and at the lab bench, to validate the molecular mechanisms involved in microbial bloom associated CaCO_3 formation in marine and lacustrine
 478 models.
 479
 480



481
 482 **Figure 8.** Conceptual diagram of proposed EPS-supported carbonate precipitation mechanism explaining the origin of whiting events.

483 **Data availability**

484 All raw data can be provided by the corresponding authors upon request.

485 **Author contributions**

486 M.M.d.B., I.B. and P.T.V. designed the study in a project directed by P.T.V., I.B. and E.V.; M.M.d.B., I.B., P.T.V., F.M., A.W. and L.P. developed the methodology;
 487 M.M.d.B. and I.B. carried out the laboratory measurements; M.M.d.B., P.T.V. and I.B. analysed the data; M.M.d.B. wrote the manuscript draft with significant
 488 contributions of P.T.V. and I.B. M.M.d.B., P.T.V., I.B., E.V., F.M., A.W and L.P. reviewed and edited the manuscript. All authors have read and agreed to the
 489 published version of the manuscript.

490 **Competing interests**

491 The authors declare that they have no conflict of interest.

492 **Acknowledgements**

493 We thank to Nelly Debrosse (Bourgogne Franche-Comté University, Dijon), Adrien Force (Bourgogne Franche-Comté University, Dijon) and Elodie Cognard
 494 (Bourgogne Franche-Comté University, Dijon) for helping with the measurements; Michel Picquet and Christine Stern (ICMUB Institut de Chimie Moléculaire,
 495 Bourgogne Franche-Comté University, Dijon, France) for their technical assistance with FT-IR analysis; Christophe Loup and Nadia Crini (Laboratoire Chrono-
 496 environnement, UMR CNRS 6249, Bourgogne Franche-Comté University, Besançon, France) for their technical assistance with Ion chromatography and ICP analyses.
 497 The authors would like to thank the reviewers whose work has helped to improve the manuscript. All individuals included in this section have consented to the
 498 acknowledgement.

499 **Financial support**

500 This study is a contribution of the SEDS and SAMBA teams of Biogeosciences laboratory (Bourgogne Franche-Comté University, Dijon, France) to the I-SITE project
501 UB18016-BGSIS.

502 **References**

- 503 Addadi, L. and Weiner, S.: Interactions between acidic proteins and crystals: stereochemical requirements in biomineralization., *Proceedings of the National Academy of Sciences*,
504 82, 4110–4114, 1985.
- 505 Agawin, N., Duarte, C., and Agustí, S.: Growth and abundance of *Synechococcus* sp. in a Mediterranean Bay: seasonality and relationship with temperature, *Mar. Ecol. Prog. Ser.*,
506 170, 45–53, <https://doi.org/10.3354/meps170045>, 1998.
- 507 Aizawa, K. and Miyachi, S.: Carbonic anhydrase and CO₂ concentrating mechanisms in microalgae and cyanobacteria, *FEMS Microbiology Letters*, 39, 215–233,
508 <https://doi.org/10.1111/j.1574-6968.1986.tb01860.x>, 1986.
- 509 Albeck, S., Aizenberg, J., Addadi, L., and Weiner, S.: Interactions of various skeletal intracrystalline components with calcite crystals, *Journal of the American Chemical Society*, 115,
510 11691–11697, 1993.
- 511 Allen, M. M.: Simple Conditions for Growth of Unicellular Blue-Green Algae on Plates 1, 2, *Journal of phycology*, 4, 1–4, 1968.
- 512 Anderson, D. M., Glibert, P. M., and Burkholder, J. M.: Harmful algal blooms and eutrophication: Nutrient sources, composition, and consequences, *Estuaries*, 25, 704–726,
513 <https://doi.org/10.1007/BF02804901>, 2002.
- 514 Babel, P. K., Kumar, J., and Chaturvedi, V.: Proteomic de-regulation in cyanobacteria in response to abiotic stresses, *Frontiers in Microbiology*, 1315, 2019.
- 515 Badger, M. R. and Andrews, T. J.: Photosynthesis and Inorganic Carbon Usage by the Marine Cyanobacterium, *Synechococcus* sp, *Plant Physiol.*, 70, 517–523,
516 <https://doi.org/10.1104/pp.70.2.517>, 1982.
- 517 Badger, M. R. and Price, G. D.: The CO₂ concentrating mechanism in cyanobacteria and microalgae, *Physiologia Plantarum*, 84, 606–615, 1992.
- 518 Badger, M. R. and Price, G. D.: The role of carbonic anhydrase in photosynthesis, *Annual review of plant biology*, 45, 369–392, 1994.
- 519 Badger, M. R., Hanson, D., and Price, G. D.: Evolution and diversity of CO₂ concentrating mechanisms in cyanobacteria, *Functional Plant Biology*, 29, 161–173, 2002.
- 520 Badger, M. R., Price, G. D., Long, B. M., and Woodger, F. J.: The environmental plasticity and ecological genomics of the cyanobacterial CO₂ concentrating mechanism, *Journal of*
521 *Experimental Botany*, 57, 249–265, <https://doi.org/10.1093/jxb/eri286>, 2006.
- 522 Bhosle, N. B., Sawant, S. S., Garg, A., and Wagh, A. B.: Isolation and Partial Chemical Analysis of Exopolysaccharides from the Marine Fouling Diatom *Navicula subinflata*, *Botanica*
523 *Marina*, 38, <https://doi.org/10.1515/botm.1995.38.1-6.103>, 1995.
- 524 Borman, A. H., Jong, E. W., Huizinga, M., Kok, D. J., Westbroek, P., and Bosch, L.: The Role in CaCO₃ Crystallization of an Acid Ca²⁺-Binding Polysaccharide Associated with
525 Cocoliths of *Emiliania huxleyi*, *Eur J Biochem*, 129, 179–183, <https://doi.org/10.1111/j.1432-1033.1982.tb07037.x>, 1982.
- 526 Braissant, O., Cailleau, G., Dupraz, C., and Verrecchia, E. P.: Bacterially induced mineralization of calcium carbonate in terrestrial environments: the role of exopolysaccharides and
527 amino acids, *Journal of Sedimentary Research*, 73, 485–490, 2003.
- 528 Braissant, O., Decho, A. W., Dupraz, C., Glunk, C., Przekop, K. M., and Visscher, P. T.: Exopolymeric substances of sulfate-reducing bacteria: interactions with calcium at alkaline
529 pH and implication for formation of carbonate minerals, *Geobiology*, 5, 401–411, 2007.
- 530 Bundeleva, I. A., Shirokova, L. S., Bénézeth, P., Pokrovsky, O. S., Kompantseva, E. I., and Balor, S.: Calcium carbonate precipitation by anoxygenic phototrophic bacteria, *Chemical*
531 *Geology*, 291, 116–131, <https://doi.org/10.1016/j.chemgeo.2011.10.003>, 2012.
- 532 Bundeleva, I. A., Shirokova, L. S., Pokrovsky, O. S., Bénézeth, P., Ménez, B., Gérard, E., and Balor, S.: Experimental modeling of calcium carbonate precipitation by cyanobacterium
533 *Gloeocapsa* sp., *Chemical Geology*, 374–375, 44–60, <https://doi.org/10.1016/j.chemgeo.2014.03.007>, 2014.
- 534 Burnap, R., Hagemann, M., and Kaplan, A.: Regulation of CO₂ Concentrating Mechanism in Cyanobacteria, *Life*, 5, 348–371, <https://doi.org/10.3390/life5010348>, 2015.
- 535 Callieri, C. and Stockner, J.: Picocyanobacteria success in oligotrophic lakes: fact or fiction?, *J Limnol*, 59, 72, <https://doi.org/10.4081/jlimnol.2000.72>, 2000.
- 536 Callieri, C., Lami, A., and Bertoni, R.: Microcolony Formation by Single-Cell *Synechococcus* Strains as a Fast Response to UV Radiation, *Appl Environ Microbiol*, 77, 7533–7540,
537 <https://doi.org/10.1128/AEM.05392-11>, 2011.
- 538 Campbell, L. and Carpenter, E. J.: Diel patterns of cell division in marine *Synechococcus* spp. (Cyanobacteria): use of the frequency of dividing cells technique to measure growth
539 rate, 1986.
- 540 Ciebiada, M., Kubiak, K., and Daroch, M.: Modifying the Cyanobacterial Metabolism as a Key to Efficient Biopolymer Production in Photosynthetic Microorganisms, *IJMS*, 21, 7204,
541 <https://doi.org/10.3390/ijms21197204>, 2020.
- 542 Clark, D. R. and Flynn, K. J.: The relationship between the dissolved inorganic carbon concentration and growth rate in marine phytoplankton, *Proc. R. Soc. Lond. B*, 267, 953–959,
543 <https://doi.org/10.1098/rspb.2000.1096>, 2000.
- 544 Coates, J.: Interpretation of infrared spectra, a practical approach, 2000.
- 545 Coello-Camba, A. and Agustí, S.: Picophytoplankton Niche Partitioning in the Warmest Oligotrophic Sea, *Front. Mar. Sci.*, 8, 651877, <https://doi.org/10.3389/fmars.2021.651877>,
546 2021.
- 547 De Philippis, R., Sili, C., and Vincenzini, M.: Response of an exopolysaccharide-producing heterocystous cyanobacterium to changes in metabolic carbon flux, *Journal of Applied*
548 *Phycology*, 8, 275–281, 1996.
- 549 De Philippis, R., Sili, C., Paperi, R., and Vincenzini, M.: Exopolysaccharide-producing cyanobacteria and their possible exploitation: a review, *Journal of Applied Phycology*, 13,
550 293–299, 2001.
- 551 Decho, A. W. and Gutierrez, T.: Microbial extracellular polymeric substances (EPSs) in ocean systems, *Frontiers in microbiology*, 8, 922, 2017.
- 552 Decho, A. W. and Kawaguchi, T.: Extracellular polymers (EPS) and calcification within modern marine stromatolites, in: *Fossil and Recent Biofilms*, Springer, 227–240, 2003.
- 553 Diaz, M. R., Eberli, G. P., Blackwelder, P., Phillips, B., and Swart, P. K.: Microbially mediated organomineralization in the formation of ooids, *Geology*, 45, 771–774,
554 <https://doi.org/10.1130/G39159.1>, 2017.
- 555 Dittrich, M. and Obst, M.: Are picoplankton responsible for calcite precipitation in lakes?, *AMBIO: A Journal of the Human Environment*, 33, 559–564, 2004.
- 556 Dittrich, M. and Sibling, S.: Calcium carbonate precipitation by cyanobacterial polysaccharides, *Geological Society, London, Special Publications*, 336, 51–63, 2010.

- 557 Dittrich, M., Müller, B., Mavrocordatos, D., and Wehrli, B.: Induced calcite precipitation by cyanobacterium *Synechococcus*, *Acta hydrochimica et hydrobiologica*, 31, 162–169, 2003.
- 558 Dokulil, M. T. and Teubner, K.: Cyanobacterial dominance in lakes, 2000.
- 559 Dubois, M., Gilles, K. A., Hamilton, J. K., Rebers, P. t, and Smith, F.: Colorimetric method for determination of sugars and related substances, *Analytical chemistry*, 28, 350–356, 1956.
- 561 Dupraz, C. and Visscher, P. T.: Microbial lithification in marine stromatolites and hypersaline mats, *Trends in microbiology*, 13, 429–438, 2005.
- 562 Dupraz, C., Reid, R. P., Braissant, O., Decho, A. W., Norman, R. S., and Visscher, P. T.: Processes of carbonate precipitation in modern microbial mats, *Earth-Science Reviews*, 96, 141–162, <https://doi.org/10.1016/j.earscirev.2008.10.005>, 2009.
- 564 Giordano, M., Beardall, J., and Raven, J. A.: CO₂ Concentrating Mechanisms in Algae: Mechanisms, Environmental Modulation, and Evolution, *Annu. Rev. Plant Biol.*, 56, 99–131, <https://doi.org/10.1146/annurev.arplant.56.032604.144052>, 2005.
- 566 Gons, H. J., Ebert, J., Hoogveld, H. L., Takkenberg, W., and Woldringh, C. J.: Observations on cyanobacterial population collapse in eutrophic lake water, 2002.
- 567 Hagström, Å., Azam, F., Andersson, A., Wikner, J., and Rassoulzadegan, F.: Microbial loop in an oligotrophic pelagic marine ecosystem: possible roles of cyanobacteria and nanoflagellates in the organic fluxes, *Mar. Ecol. Prog. Ser.*, 49, 171–178, <https://doi.org/10.3354/meps049171>, 1988.
- 569 Havens, K. E.: Chapter 33: Cyanobacteria blooms: effects on aquatic ecosystems, 2008.
- 570 Hein, M.: Inorganic carbon limitation of photosynthesis in lake phytoplankton, *Freshwater Biology*, 37, 545–552, <https://doi.org/10.1046/j.1365-2427.1997.00180.x>, 1997.
- 571 Heisler, J., Glibert, P. M., Burkholder, J. M., Anderson, D. M., Cochlan, W., Dennison, W. C., Dortch, Q., Gobler, C. J., Heil, C. A., Humphries, E., Lewitus, A., Magnien, R., Marshall, H. G., Sellner, K., Stockwell, D. A., Stoecker, D. K., and Suddleson, M.: Eutrophication and harmful algal blooms: A scientific consensus, *Harmful Algae*, 8, 3–13, <https://doi.org/10.1016/j.hal.2008.08.006>, 2008.
- 574 Hodell, D. A., Schelske, C. L., Fahnenstiel, G. L., and Robbins, L. L.: Biologically induced calcite and its isotopic composition in Lake Ontario, *Limnology and Oceanography*, 43, 187–199, 1998.
- 576 Huisman, J., Codd, G. A., Paerl, H. W., Ibelings, B. W., Verspagen, J. M. H., and Visser, P. M.: Cyanobacterial blooms, *Nat Rev Microbiol*, 16, 471–483, <https://doi.org/10.1038/s41579-018-0040-1>, 2018.
- 578 Ibelings, B. W. and Maberly, S. C.: Photoinhibition and the availability of inorganic carbon restrict photosynthesis by surface blooms of cyanobacteria, *Limnology and Oceanography*, 43, 408–419, 1998a.
- 580 Ionescu, D., Spitzer, S., Reimer, A., Schneider, D., Daniel, R., Reitner, J., de Beer, D., and Arp, G.: Calcium dynamics in microbialite-forming exopolymer-rich mats on the atoll of Kiritimati, Republic of Kiribati, Central Pacific, *Geobiology*, 13, 170–180, <https://doi.org/10.1111/gbi.12120>, 2015.
- 582 Kamennaya, N., Ajo-Franklin, C., Northen, T., and Jansson, C.: Cyanobacteria as Biocatalysts for Carbonate Mineralization, *Minerals*, 2, 338–364, <https://doi.org/10.3390/min2040338>, 2012.
- 584 Kansiz, M., Heraud, P., Wood, B., Burden, F., Beardall, J., and McNaughton, D.: Fourier Transform Infrared microspectroscopy and chemometrics as a tool for the discrimination of cyanobacterial strains, *Phytochemistry*, 52, 407–417, [https://doi.org/10.1016/S0031-9422\(99\)00212-5](https://doi.org/10.1016/S0031-9422(99)00212-5), 1999.
- 586 Kavita, K., Mishra, A., and Jha, B.: Isolation and physico-chemical characterisation of extracellular polymeric substances produced by the marine bacterium *Vibrio parahaemolyticus*, *Biofouling*, 27, 309–317, <https://doi.org/10.1080/08927014.2011.562605>, 2011.
- 588 Kawaguchi, T. and Decho, A. W.: Isolation and biochemical characterization of extracellular polymeric secretions (EPS) from modern soft marine stromatolites (Bahamas) and its inhibitory effect on CaCO₃ precipitation, *Preparative Biochemistry and Biotechnology*, 32, 51–63, 2002.
- 590 Kieft, B., Li, Z., Bryson, S., Hettich, R. L., Pan, C., Mayali, X., and Mueller, R. S.: Phytoplankton exudates and lysates support distinct microbial consortia with specialized metabolic and ecophysiological traits, *Proc. Natl. Acad. Sci. U.S.A.*, 118, e2101178118, <https://doi.org/10.1073/pnas.2101178118>, 2021.
- 592 Kjelleberg, S., Hermansson, M., Marden, P., & Jones, G. W.: The transient phase between growth and non-growth of heterotrophic bacteria, with emphasis on the marine environment, *Annual Reviews in Microbiology*, 41(1), 25-49, 1987.
- 594
- 595 Kupriyanova, E. V. and Pronina, N. A.: Carbonic anhydrase: Enzyme that has transformed the biosphere, *Russ J Plant Physiol*, 58, 197–209, <https://doi.org/10.1134/S1021443711020099>, 2011.
- 597 Kupriyanova, E. V., Sinetova, M. A., Bedbenov, V. S., Pronina, N. A., and Los, D. A.: Putative extracellular α -Class carbonic anhydrase, EcaA, of *Synechococcus elongatus* PCC 7942 is an active enzyme: A sequel to an old story, *Microbiology*, 164, 576–586, 2018.
- 599 Lange, N. A.: Lange's handbook of chemistry, 15. ed., edited by: Dean, J. A., McGraw-Hill, New York, NY, 1999.
- 600 Larson, E. B. and Mylroie, J. E.: A review of whiting formation in the Bahamas and new models, *Carbonates and Evaporites*, 29, 337–347, 2014.
- 601 Liu, L., Huang, Q., and Qin, B.: Characteristics and roles of *Microcystis* extracellular polymeric substances (EPS) in cyanobacterial blooms: a short review, *Journal of Freshwater Ecology*, 33, 183–193, <https://doi.org/10.1080/02705060.2017.1391722>, 2018.
- 602
- 603 Lürling, M., Mello, M. M. e, van Oosterhout, F., de Senerpont Domis, L., and Marinho, M. M.: Response of Natural Cyanobacteria and Algae Assemblages to a Nutrient Pulse and Elevated Temperature, *Front. Microbiol.*, 9, 1851, <https://doi.org/10.3389/fmicb.2018.01851>, 2018.
- 604
- 605 Maberly, S. C.: Diel, episodic and seasonal changes in pH and concentrations of inorganic carbon in a productive lake, *Freshwater Biology*, 35, 579–598, <https://doi.org/10.1111/j.1365-2427.1996.tb01770.x>, 1996.
- 606
- 607 Maeda, H., Kawai, A., and Tilzer, M. M.: The water bloom of Cyanobacterial picoplankton in Lake Biwa, Japan, *Hydrobiologia*, 248, 93–103, <https://doi.org/10.1007/BF00006077>, 1992.
- 608
- 609 Marin, F., Corstjens, P., de Gaulejac, B., de Vrind-De Jong, E., and Westbroek, P.: Mucins and molluscan calcification: molecular characterization of mucoperlin, a novel mucin-like protein from the nacreous shell layer of the fan mussel *Pinna nobilis* (Bivalvia, Pteriomorpha), *Journal of Biological Chemistry*, 275, 20667–20675, 2000.
- 610
- 611 Martinez, R. E., Gardés, E., Pokrovsky, O. S., Schott, J., and Oelkers, E. H.: Do photosynthetic bacteria have a protective mechanism against carbonate precipitation at their surfaces?, *Geochimica et Cosmochimica Acta*, 74, 1329–1337, <https://doi.org/10.1016/j.gca.2009.11.025>, 2010.
- 612
- 613 Martinho de Brito, M., Bundeleva, I., Marin, F., Vennin, E., Wilton, A., Plasseraud, L., and Visscher, P. T.: Effect of Culture pH on Properties of Exopolymeric Substances from *Synechococcus* PCC7942: Implications for Carbonate Precipitation, *Geosciences*, 12, 210, <https://doi.org/10.3390/geosciences12050210>, 2022.
- 614
- 615 Marvasi, M., Visscher, P. T., and Casillas Martinez, L.: Exopolymeric substances (EPS) from *Bacillus subtilis*: polymers and genes encoding their synthesis, *FEMS microbiology letters*, 313, 1–9, 2010.
- 616
- 617 Mayo, W. P., Elrifi, I. R., and Turpin, D. H.: The Relationship between Ribulose Bisphosphate Concentration, Dissolved Inorganic Carbon (DIC) Transport and DIC-Limited Photosynthesis in the Cyanobacterium *Synechococcus leopoliensis* Grown at Different Concentrations of Inorganic Carbon, *Plant Physiol.*, 90, 720–727, <https://doi.org/10.1104/pp.90.2.720>, 1989.
- 618
- 619

- 620 Miller, A. G., Turpin, D. H., and Canvin, D. T.: Growth and Photosynthesis of the Cyanobacterium *Synechococcus leopoliensis* in HCO₃⁻ Limited Chemostats, *Plant Physiol.*, 75,
621 1064–1070, <https://doi.org/10.1104/pp.75.4.1064>, 1984.
- 622 Mitterer, R. M. and Cunningham, R.: The interaction of natural organic matter with grain surfaces: implications for calcium carbonate precipitation, 1985.
- 623 Murphy, L. S. and Haugen, E. M.: The distribution and abundance of phototrophic ultraplankton in the North Atlantic 1,2: Phototrophic ultraplankton, *Limnol. Oceanogr.*, 30, 47–58,
624 <https://doi.org/10.4319/lo.1985.30.1.0047>, 1985.
- 625 Myklestad, S. and Haug, A.: Concentration of Nutrients in Culture Medium, 1972.
- 626 Myklestad, S., Holm-Hansen, O., Vårum, K. M., and Volcani, B. E.: Rate of release of extracellular amino acids and carbohydrates from the marine diatom *Chaetoceros affinis*, *J*
627 *Plankton Res.*, 11, 763–773, <https://doi.org/10.1093/plankt/11.4.763>, 1989.
- 628 Obst, M., Dynes, J. J., Lawrence, J. R., Swerhone, G. D., Benzerara, K., Karunakaran, C., Kaznatcheev, K., Tylliszczak, T., and Hitchcock, A. P.: Precipitation of amorphous CaCO₃
629 (aragonite-like) by cyanobacteria: a STXM study of the influence of EPS on the nucleation process, *Geochimica et Cosmochimica Acta*, 73, 4180–4198, 2009.
- 630 O’Neil, J. M., Davis, T. W., Burford, M. A., and Gobler, C. J.: The rise of harmful cyanobacteria blooms: The potential roles of eutrophication and climate change, *Harmful Algae*,
631 14, 313–334, <https://doi.org/10.1016/j.hal.2011.10.027>, 2012.
- 632 Paerl, H.: Chapter 10: Nutrient and other environmental controls of harmful cyanobacterial blooms along the freshwater–marine continuum, 2008.
- 633 Paerl, H. W. and Huisman, J.: Blooms Like It Hot, *Science*, 320, 57–58, <https://doi.org/10.1126/science.1155398>, 2008.
- 634 Paerl, H. W., Fulton, R. S., Moisander, P. H., and Dyble, J.: Harmful Freshwater Algal Blooms, With an Emphasis on Cyanobacteria, *The Scientific World JOURNAL*, 1, 76–113,
635 <https://doi.org/10.1100/tsw.2001.16>, 2001.
- 636 Palenik, B.: Chromatic Adaptation in Marine *Synechococcus* Strains, *Appl Environ Microbiol.*, 67, 991–994, <https://doi.org/10.1128/AEM.67.2.991-994.2001>, 2001.
- 637 Pannard, A., Pédrone, J., Bormans, M., Briand, E., Claquin, P., and Lagadeuc, Y.: Production of exopolymers (EPS) by cyanobacteria: impact on the carbon-to-nutrient ratio of the
638 particulate organic matter, *Aquat Ecol.*, 50, 29–44, <https://doi.org/10.1007/s10452-015-9550-3>, 2016.
- 639 Pereira, S., Zille, A., Micheletti, E., Moradas-Ferreira, P., De Philippis, R., and Tamagnini, P.: Complexity of cyanobacterial exopolysaccharides: composition, structures, inducing
640 factors and putative genes involved in their biosynthesis and assembly, *FEMS microbiology reviews*, 33, 917–941, 2009.
- 641 Philips, E. J., Badylak, S., and Lynch, T. C.: Blooms of the picoplanktonic cyanobacterium *Synechococcus* in Florida Bay, a subtropical inner-shelf lagoon, *Limnol. Oceanogr.*, 44,
642 1166–1175, <https://doi.org/10.4319/lo.1999.44.4.1166>, 1999.
- 643 Ploug, H.: Cyanobacterial surface blooms formed by *Aphanizomenon* sp. and *Nodularia spumigena* in the Baltic Sea: Small-scale fluxes, pH, and oxygen microenvironments, *Limnol.*
644 *Oceanogr.*, 53, 914–921, <https://doi.org/10.4319/lo.2008.53.3.0914>, 2008.
- 645 Pomar, L. and Hallock, P.: Carbonate factories: a conundrum in sedimentary geology, *Earth-Science Reviews*, 87, 134–169, 2008.
- 646 Price, G. D.: Inorganic carbon transporters of the cyanobacterial CO₂ concentrating mechanism, *Photosynth Res.*, 109, 47–57, <https://doi.org/10.1007/s11120-010-9608-y>, 2011.
- 647 Price, G. D., Badger, M. R., Woodger, F. J., and Long, B. M.: Advances in understanding the cyanobacterial CO₂-concentrating-mechanism (CCM): functional components, Ci
648 transporters, diversity, genetic regulation and prospects for engineering into plants, *Journal of Experimental Botany*, 59, 1441–1461, <https://doi.org/10.1093/jxb/erm112>, 2008.
- 649 Price, G. D., Maeda, S., Omata, T., and Badger, M. R.: Modes of active inorganic carbon uptake in the cyanobacterium, *Synechococcus* sp. PCC7942, *Functional Plant Biol.*, 29, 131,
650 <https://doi.org/10.1071/PP01229>, 2002.
- 651 Price, G. D., Sültemeyer, D., Klughammer, B., Ludwig, M., and Badger, M. R.: The functioning of the CO₂ concentrating mechanism in several cyanobacterial strains: a review of
652 general physiological characteristics, genes, proteins, and recent advances, *Canadian Journal of Botany*, 76, 973–1002, 1998.
- 653 Rae, B. D., Long, B. M., Whitehead, L. F., Förster, B., Badger, M. R., and Price, G. D.: Cyanobacterial Carboxysomes: Microcompartments that Facilitate CO₂ Fixation, *Microb*
654 *Physiol.*, 23, 300–307, <https://doi.org/10.1159/000351342>, 2013.
- 655 Raven, J. A., Beardall, J., and Sánchez-Baracaldo, P.: The possible evolution and future of CO₂-concentrating mechanisms, *Journal of Experimental Botany*, 68, 3701–3716, 2017.
- 656 Reynolds, C. S.: Cyanobacterial Water-Blooms, in: *Advances in Botanical Research*, vol. 13, Elsevier, 67–143, [https://doi.org/10.1016/S0065-2296\(08\)60341-9](https://doi.org/10.1016/S0065-2296(08)60341-9), 1987.
- 657 Reynolds, C. S. and Walsby, A. E.: WATER-BLOOMS, *Biological Reviews*, 50, 437–481, <https://doi.org/10.1111/j.1469-185X.1975.tb01060.x>, 1975.
- 658 Rippka, R., Deruelles, J., Waterbury, J. B., Herdman, M., and Stanier, R. Y.: Generic assignments, strain histories and properties of pure cultures of cyanobacteria, *Microbiology*, 111,
659 1–61, 1979.
- 660 Robbins, L. and Blackwelder, P.: Biochemical and ultrastructural evidence for the origin of whittings: A biologically induced calcium carbonate precipitation mechanism, *Geology*,
661 20, 464–468, 1992.
- 662 Rossi, F. and De Philippis, R.: Role of cyanobacterial exopolysaccharides in phototrophic biofilms and in complex microbial mats, *Life*, 5, 1218–1238, 2015.
- 663 Sandrini, G., Tann, R. P., Schuurmans, J. M., van Beusekom, S. A. M., Matthijs, H. C. P., and Huisman, J.: Diel Variation in Gene Expression of the CO₂-Concentrating Mechanism
664 during a Harmful Cyanobacterial Bloom, *Front. Microbiol.*, 7, <https://doi.org/10.3389/fmicb.2016.00551>, 2016.
- 665 Schultze-Lam, S., Harauz, G., and Beveridge, T. J.: Participation of a cyanobacterial S layer in fine-grain mineral formation, *J Bacteriol.*, 174, 7971–7981,
666 <https://doi.org/10.1128/jb.174.24.7971-7981.1992>, 1992.
- 667 Schultze-Lam, S., Schultze-Lam, S., Beveridge, T. J., and Des Marais, D. J.: Whiting events: biogenic origin due to the photosynthetic activity of cyanobacterial picoplankton,
668 *Limnology and oceanography*, 42, 133–141, 1997.
- 669 Shinn, E. A., Steinen, R. P., Lidz, B. H., and Swart, P. K.: Whittings, a sedimentologic dilemma, *Journal of Sedimentary Research*, 59, 147–161, 1989.
- 670 Skoog, E. J., Moore, K. R., Gong, J., Ciccarese, D., Momper, L., Cutts, E. M., and Bosak, T.: Metagenomic, (bio)chemical, and microscopic analyses reveal the potential for the
671 cycling of sulfated EPS in Shark Bay pustular mats, *ISME COMMUN.*, 2, 43, <https://doi.org/10.1038/s43705-022-00128-1>, 2022.
- 672 Stal, L., Van Gemerden, H., and Krumbein, W.: The simultaneous assay of chlorophyll and bacteriochlorophyll in natural microbial communities, *Journal of microbiological methods*,
673 2, 295–306, 1984.
- 674 Stanton, C., Barnes, B. D., Kump, L. R., and Cosmidis, J.: A re-examination of the mechanism of whiting events: A new role for diatoms in Fayetteville Green Lake (New York,
675 USA), *Geobiology*, 2021.
- 676 Tai, V. and Palenik, B.: Temporal variation of *Synechococcus* clades at a coastal Pacific Ocean monitoring site, *ISME J.*, 3, 903–915, <https://doi.org/10.1038/ismej.2009.35>, 2009.
- 677 Takahashi, Y., Yamaguchi, O., and Omata, T.: Roles of CmpR, a LysR family transcriptional regulator, in acclimation of the cyanobacterium *Synechococcus* sp. strain PCC 7942 to
678 low-CO₂ and high-light conditions: High-light and low-CO₂ acclimation in cyanobacteria, *Molecular Microbiology*, 52, 837–845, <https://doi.org/10.1111/j.1365-2958.2004.04021.x>,
679 2004.

- 680 Talling, J. F.: The Depletion of Carbon Dioxide from Lake Water by Phytoplankton, *The Journal of Ecology*, 64, 79, <https://doi.org/10.2307/2258685>, 1976.
- 681 Thompson, J. B.: Microbial whittings, *Microbial sediments*, 250–260, 2000.
- 682 Thompson, J. and Ferris, F.: Cyanobacterial precipitation of gypsum, calcite, and magnesite from natural alkaline lake water, *Geology*, 18, 995–998, 1990.
- 683 Thompson, J. B., Ferris, F. G., and Smith, D. A.: Geomicrobiology and Sedimentology of the Mixolimnion and Chemocline in Fayetteville Green Lake, New York, *PALAIOS*, 5, 52,
684 <https://doi.org/10.2307/3514996>, 1990.
- 685 Tortell, P. D.: Evolutionary and ecological perspectives on carbon acquisition in phytoplankton, *Limnol. Oceanogr.*, 45, 744–750, <https://doi.org/10.4319/lo.2000.45.3.0744>, 2000.
- 686 Tortell, P. D., Rau, G. H., and Morel, F. M. M.: Inorganic carbon acquisition in coastal Pacific phytoplankton communities, *Limnol. Oceanogr.*, 45, 1485–1500,
687 <https://doi.org/10.4319/lo.2000.45.7.1485>, 2000.
- 688 Townsend, D. W., Cammen, L. M., Holligan, P. M., Campbell, D. E., and Pettigrew, N. R.: Causes and consequences of variability in the timing of spring phytoplankton blooms,
689 *Deep Sea Research Part I: Oceanographic Research Papers*, 41, 747–765, [https://doi.org/10.1016/0967-0637\(94\)90075-2](https://doi.org/10.1016/0967-0637(94)90075-2), 1994.
- 690 Trichet, J. and Defarge, C.: Non-biologically supported organomineralization, *Bulletin-Institut Oceanographic Monaco-Numero Special-*, 203–236, 1995.
- 691 Verspagen, J. M. H., Van de Waal, D. B., Finke, J. F., Visser, P. M., Van Donk, E., and Huisman, J.: Rising CO₂ Levels Will Intensify Phytoplankton Blooms in Eutrophic and
692 Hypertrophic Lakes, *PLoS ONE*, 9, e104325, <https://doi.org/10.1371/journal.pone.0104325>, 2014.
- 693 Visscher, P. T., Reid, R. P., Bebout, B. M., Hoefft, S. E., Macintyre, I. G., & Thompson, J. A.: Formation of lithified micritic laminae in modern marine stromatolites (Bahamas); the
694 role of sulfur cycling. *American Mineralogist*, 83(11-12_Part_2), 1482-1493, 1998.
- 695
- 696 Walker, J. M., Marzec, B., Lee, R. B. Y., Vodrazkova, K., Day, S. J., Tang, C. C., Rickaby, R. E. M., and Nudelman, F.: Polymorph Selectivity of Coccolith-Associated Polysaccharides
697 from *Gephyrocapsa Oceanica* on Calcium Carbonate Formation In Vitro, *Adv. Funct. Mater.*, 29, 1807168, <https://doi.org/10.1002/adfm.201807168>, 2019.
- 698 Wall, R. S. and Gyi, T. J.: Alcian blue staining of proteoglycans in polyacrylamide gels using the “critical electrolyte concentration” approach, *Analytical biochemistry*, 175, 298–299,
699 1988.
- 700 Wang, L.-L., Wang, L.-F., Ren, X.-M., Ye, X.-D., Li, W.-W., Yuan, S.-J., Sun, M., Sheng, G.-P., Yu, H.-Q., and Wang, X.-K.: pH dependence of structure and surface properties of
701 microbial EPS, *Environmental science & technology*, 46, 737–744, 2012.
- 702 Weisse, T.: Dynamics of Autotrophic Picoplankton in Marine and Freshwater Ecosystems, in: *Advances in Microbial Ecology*, vol. 13, edited by: Jones, J. G., Springer US, Boston,
703 MA, 327–370, https://doi.org/10.1007/978-1-4615-2858-6_8, 1993.
- 704 Wells, A. J. and Iling, L. V.: Present-Day Precipitation of Calcium Carbonate in the Persian Gulf, 1964.
- 705 Wheeler, A., George, J. W., and Evans, C.: Control of calcium carbonate nucleation and crystal growth by soluble matrix of oyster shell, *Science*, 212, 1397–1398, 1981.
- 706 Whitton, B. A. and Potts, M.: Introduction to the Cyanobacteria, in: *Ecology of Cyanobacteria II*, edited by: Whitton, B. A., Springer Netherlands, Dordrecht, 1–13,
707 https://doi.org/10.1007/978-94-007-3855-3_1, 2012.
- 708 Xu, H., Paerl, H. W., Qin, B., Zhu, G., Hall, N. S., and Wu, Y.: Determining Critical Nutrient Thresholds Needed to Control Harmful Cyanobacterial Blooms in Eutrophic Lake Taihu,
709 China, *Environ. Sci. Technol.*, 49, 1051–1059, <https://doi.org/10.1021/es503744q>, 2015.
- 710 Yang, G., Li, F., Deng, Z., Wang, Y., Su, Z., Huang, L., Yin, L., and Ji, C.: Abnormal Crystallization Sequence of Calcium Carbonate in the Presence of *Synechococcus* sp. PCC 7942,
711 *Geomicrobiology Journal*, 40, 34–45, <https://doi.org/10.1080/01490451.2022.2100948>, 2023.
- 712 Yates, K. K. and Robbins, L. L.: Production of carbonate sediments by a unicellular green alga, *American Mineralogist*, 83, 1503–1509, 1998.
- 713 Zepernick, B. N., Gann, E. R., Martin, R. M., Pound, H. L., Krausfeldt, L. E., Chaffin, J. D., and Wilhelm, S. W.: Elevated pH Conditions Associated With *Microcystis* spp. Blooms
714 Decrease Viability of the Cultured Diatom *Fragilaria crotonensis* and Natural Diatoms in Lake Erie, *Frontiers in microbiology*, 12, 188, 2021.
- 715 Zhao, H., Han, G., Zhang, S., and Wang, D.: Two phytoplankton blooms near Luzon Strait generated by lingering Typhoon Parma: Lingering Typhoon-Induced Algae Blooms, *J.*
716 *Geophys. Res. Biogeosci.*, 118, 412–421, <https://doi.org/10.1002/jgrg.20041>, 2013.
- 717